Preprints.org

Article

Not peer-reviewed version

Getting Enhanced Catalytic Surfaces for Catechol Sensing! Combination of Grafted Aryldiazonium Derivative and Either Cross-Linking Dopamine or Coupling Tyrosinase Immobilizations

Javier M. González-Costas , Sara Caruncho-Pérez , Elisa González-Romero *

Posted Date: 21 February 2025

doi: 10.20944/preprints202502.1766.v1

Keywords: aryldiazonium ions; (bio)sensor; dopamine; catechol; tyrosinase; Raman; voltammetry

Preprints.org is a free multidisciplinary platform providing preprint service that is dedicated to making early versions of research outputs permanently available and citable. Preprints posted at Preprints.org appear in Web of Science, Crossref, Google Scholar, Scilit, Europe PMC.

Copyright: This open access article is published under a Creative Commons CC BY 4.0 license, which permit the free download, distribution, and reuse, provided that the author and preprint are cited in any reuse.

Preprints.org (www.preprints.org) | NOT PEER-REVIEWED | Posted: 21 February 2025 doi:10.20944/preprints202502.1766.v1

Disclaimer/Publisher's Note: The statements, opinions, and data contained in all publications are solely those of the individual author(s) and contributor(s) and not of MDPI and/or the editor(s). MDPI and/or the editor(s) disclaim responsibility for any injury to people or property resulting from any ideas, methods, instructions, or products referred to in the content.

Article

Getting Enhanced Catalytic Surfaces for Catechol Sensing! Combination of Grafted Aryldiazonium Derivative and Either Cross-Linking Dopamine or Coupling Tyrosinase Immobilizations

Javier Marcos González-Costas, Sara Caruncho-Pérez and Elisa González-Romero*

[1] Department of Analytical and Food Chemistry, Universidade de Vigo, University of Vigo, Campus Lagoas-Marcosende, Vigo, 36310, Spain

* Correspondence: eromero@uvigo.es; Tel.: +34 986812240

Abstract: The research work presented here describes the development of catalytic surfaces immobilizing dopamine via cross-linking or tyrosinase via covalent bond on an electrografted screen-printed carbon electrode with a 4-nitrobenzenediazonium ion. A simple electrochemical reduction approach was used to graft aryldiazonium ions onto commercial electrodes, resulting in the formation of a covalently bonded aromatic layer on the electrode surface. After functionalization with aminophenyl groups, dopamine, an important neurotransmitter, was immobilized by imine bond formation using glutaraldehyde as a bifunctional cross-linking molecule. The presence of immobilized dopamine was confirmed by cyclic voltammetry following the electrochemical response of the hydroquinone/quinone redox process from catechol functionalities on the surface, which are responsible for the catalytic activity. In addition, the surface was also characterized by cyclic voltammetry using the redox probe, $[Fe(CN)_6]^{3-/4-}$, obtaining a signal on this catalytic DA-biosensor about 14 times higher than that of a bare electrode, achieving a dynamic concentration range spanning three orders of magnitude. Remarkable sensitivity was also obtained by combining the electrografting, *in situ* diazotation to generate grafted aryl diazonium ions on the surface and coupling reaction to anchor the tyrosinase enzyme to the electrode surface. The response of the TYR-biosensor towards catechol, using the redox probe as mediator, was 10 times higher than that obtained with the dopamine modified catalytic surface. These modified surfaces offer promising alternatives for the voltammetric quantification of catechol in environmental fields.

Keywords: aryldiazonium ions; (bio)sensor; dopamine; catechol; tyrosinase; Raman; voltammetry

1. Introduction

Over the past decade, the interest of the scientific community in the electrografting of aromatic diazonium salts has increased notably [1,2]. This interest is attributable to the stability and reproducibility of the covalent bond formed between the organic layer and the electrode surface [3–6]. Specifically, electrochemical grafting of aryldiazonium salts represents a rapid, straightforward and versatile methodology for surface modification. The formation of a thin or thick film can be controlled by varying the electrografting conditions (cathodic potential, scan rate and number of scans), the concentration of the aryldiazonium salt, the use of aqueous or organic solvents, the temperature and the reaction time [7–11].

The use of aryldiazonium salts represents an elegant approach to modify a range of conductive substrates, including carbon [12] (glassy carbon [13], HOPG [14], graphene [15], diamond [16], carbon nanotubes [17]), metals (Au [18], Ni [19], Fe [20] and Pt [21]), semiconductors (Si [22] and BDD [23]) and other conductive polymeric surfaces (PEDOT [24] and ITO [25]). The grafted species can carry a variety of functional groups depending on the target applications, such as the detection of molecules

© 2025 by the author(s). Distributed under a Creative Commons CC BY license.

Preprints.org (www.preprints.org) | NOT PEER-REVIEWED | Posted: 21 February 2025 doi:10.20944/preprints202502.1766.v1

of biomedical, environmental or food interest. Consequently, these organic layers are useful for the covalent immobilization of biological molecules (antibodies, DNA, enzymes, neurotransmitters and toxins) in the design of electrochemical sensors [1,26,27].

Tyrosinase (TYR) is a polyphenol oxidase enzyme with an active site consisting of two copper atoms, which are coordinated to six histidine residues, and is stabilized by disulphide bonds [28]. From clinical point of view, TYR enables catecholase activities, being involved in catecholamine's physiological processes in the human body that can influence human health. Moreover, this metalloenzyme plays a role in melanogenesis, acting as a catalyst in the biosynthesis of melanin pigments found in human skin and hair. Briefly, in the presence of molecular oxygen as cofactor, TYR initially hydroxylates monophenolic substrates to produce o-diphenols, which are then oxidized to form o-quinones [29,30]. For decades and widely described in the bibliography [31–36], many authors have used its versatile catalytic properties in the field of electrochemical biosensors development for either point-of-care testing of catecholamines or portable monitoring devices for phenolic detection, but it has also revealed as a promising molecule for biotechnological applications in environmental remediation [28].

As stated above, one substrate of TYR is the catecholamine called dopamine (DA) that plays an important role in the nervous system (neurotransmitter), influencing a multitude of functions such as motor activity, learning, mood and attention span. DA has been extensively studied by electrochemical methods due to its electroactive 1,2-dihydroxyphenyl groups and the terminal amino group which allows the formation of covalent bonds [37]. The interest shown by the scientific community towards this molecule is double; firstly, its analysis and monitoring in biological fluids by TYR-enzyme biosensors [38,39] and, secondly, its use as modifier in the design of biosensors for the determination of other relevant molecules. Several methods for the immobilization of DA on surfaces can be found in the literature [40–43].

In this context, the present study (based on a granted Patent [44]) focused on the grafting of organic monolayers by the electrochemical reduction of 4-nitrobenzenediazonium ions (4-NBD^+) onto a screen-printed electrode (SPE). To confirm that the grafting was successful, voltammetric and spectroscopic techniques were used. Subsequently, two strategies were developed using this grafted platform. In the first one, DA was covalently immobilized on the aminophenyl-functionalized screen-printed carbon electrode (SPCE) with glutaraldehyde (GLU) as a cross-linking molecule. The electrochemical activity of the DA-modified surface was characterized by cyclic voltammetry (CV) using potassium ferricyanide ($K_3[Fe(CN)_6]$) and catechol (CC) solutions. The redox behavior of the modified electrode was analyzed to confirm the successful functionalization and to evaluate its electrocatalytic potential. The second strategy takes advantage of the rich chemistry of arenediazonium salts by modifying the grafted surface by *in situ* diazotization of aminophenyl groups to obtain aryldiazonium ions on it. These generated diazonium ions will be responsible for immobilizing the TYR enzyme through a coupling reaction where the phenolic residues of the enzyme covalently bind via azo group (-N=N-) formation. Finally, due to the relevance of catechol detection in environmental applications, the response of the developed (bio)sensors to this phenolic contaminant and their comparison were investigated.

2. Materials and Methods

2.1. Reagents and Solution

4-Nitrobenzenediazonium tetrafluoroborate, 4-NBD^+, (MW 236.92 g mol^{-1}, 97 %), GLU (1.06 g mL^{-1}, 25 %), CC (> 99 %), DA (98 %), potassium ferricyanide (99 %) and Tyrosinase (1,000 U mg^{-1}) (EC 1.14.18.1) from mushroom were supplied by Sigma-Aldrich (Burlington, MA, USA). Hydrochloric acid (37 %) and sulphuric acid (96 %) were acquired from Fluka (Nueva Jersey, USA). Phosphate-buffered solution (PBS) was prepared with mono and dibasic potassium phosphate (> 99 %) and TRIS-buffered solution with 2-Amino-2-(hidroximetil)-1,3-propanodiol; the three reagents were supplied from Panreac (Barcelona, Spain). The pH of PBS or TRIS was measured and adjusted using

Preprints.org (www.preprints.org) | NOT PEER-REVIEWED | Posted: 21 February 2025 doi:10.20944/preprints202502.1766.v1

NaOH or HCl (Metrohm Hispania 744 pH-meter, Spain), which were used as a supporting electrolyte and medium for coupling reaction, respectively. Sodium nitrite (> 99 %) and sodium hydroxide (99 %) were purchased from Riedel-de-Haën. All chemicals were acquired at the highest purity available and used without further purification. Stock standard solutions of the 4-NBD$^+$ were prepared daily in 1 M HCl and stored in the dark at temperatures close to 0°C to minimize diazotate formation [45]. Ultrapure water was obtained by the reverse osmosis RO1-Compact/C and UV system (κ= 1.2 µS cm^{-1}) (Peter Taboada, Spain).

2.2. Instrumentation

Cyclic voltammetric measurements were carried out using an Autolab PGSTAT 30 potentiostat from Eco-Chemie (KM Utrecht, The Netherlands), controlled by the GPES 4.9 (General Purpose Electrochemical Experiments) software package and a µStat-100 potentiostat from DropSens (Metrohm-DropSens, Oviedo, Spain), controlled by the PSLite (PalmSens, CL Houten, The Netherlands) software. A SPE (0.126 cm^2 geometric area) from Metrohm-Dropsens was employed as a miniaturized equivalent of a traditional electrochemical cell. The SPE comprised three electrodes printed on a ceramic substrate: a working electrode (carbon, carbon modified with Multiwalled Carbon Nanotubes, MWCNTs, or gold), a silver pseudoreference electrode and an auxiliary electrode (carbon or gold). In this experimental work, carbon (SPCE), carbon modified with Multiwalled Carbon Nanotubes (MWCNT-SPCE) and gold with high temperature (AuAT-SPE) and low temperature (AuBT-SPE) cured inks SPEs were used. The SPE was connected to the potentiostat via a SPE connector (Metrohm-Dropsens), which served as an interface, and it was placed inside a Faraday cage.

Surface-enhanced Raman spectroscopy (SERS) measurements were performed using an inVia Reflex Raman spectrometer coupled to a confocal microscope (Renishaw) and a 2D-CCD camera. Raman spectra were recorded in the range of 200 to 1800 cm^{-1}, employing a 785 nm excitation laser, a 20x objective lens and an accumulation time of 10 seconds.

2.3. Electrochemical Measurements

The voltammetric measurements were performed at room temperature by applying a 50 µL drop of solution onto the SPE, ensuring that all three electrodes were completely covered. The modified surfaces were electrochemically characterized by CV using 1 mM $[Fe(CN)_6]^{3-/4-}$ in 50 mM PBS at pH 7.4, with a potential window of +0.5 V to -0.5 V (starting potential at +0.5 V or -0.5 V according to convenience) at a scan rate of 100 mVs^{-1} (unless otherwise indicated). DA-immobilized surface was also characterized by CV employing 50 mM PBS at pH 7.4, in the absence and presence of 3 mM CA, and applied a potential window from -0.5 V to +1.0 V at a scan rate of 100 mVs^{-1}.

2.4. Procedures

2.4.1. Electrografting of 4-NBD$^+$ on SPE

Prior to the grafting step, the SPEs were electrochemically activated in acidic media. Activation of the MWCNT-SPCEs and SPCEs was performed by CV using 50 µL of 0.1 M H_2SO_4, applied during 5 consecutive potential scans from +0.5 V to -1.5 V *vs*. Ag pseudoreference electrode at a scan rate of 100 mVs^{-1}. Similarly, the gold electrodes were activated by CV with 50 µL of 0.1 M H_2SO_4, applying 10 continuous potential scans from -0.5V to +1.5 V at the same scanning rate. The electrodes were then rinsed with Milli-Q water and dried with an air stream.

After activation, the MWCNT-SPCEs and SPCEs were electrografted with 50 µL of a 2 mM 4-NBD$^+$ solution prepared in 25 mM HCl (Figure 1). CV was then employed to reduce the 4-NBD$^+$ ions in the potential window from +0.5 V to -1.0 V for 5 cycles at a scan rate of 100 mVs^{-1}. The surface was then rinsed with 25 mM HCl and dried using an air stream. For the AuAT-SPE and AuBT-SPE, the electrochemical reduction of the 2 mM 4-NBD$^+$ in 25 mM HCl was carried out in the potential window

Preprints.org (www.preprints.org) | NOT PEER-REVIEWED | Posted: 21 February 2025 doi:10.20944/preprints202502.1766.v1

from 0.5 to -0.5 V for 5 cycles at a scan rate of 100 mVs^{-1}. The grafted surfaces were labelled as SPE-GRAFT.

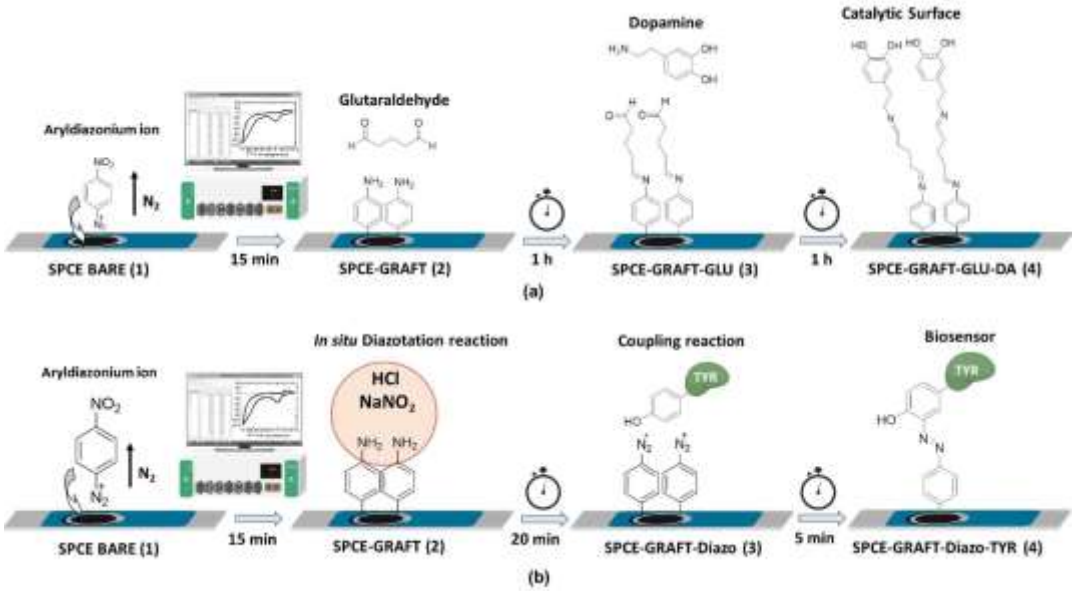

Figure 1. Schemes illustrating the development of (a) the catalytic surface SPCE-GRAFT-GLU-DA (DA-biosensor) and (b) the enzyme electrode by TYR immobilization, named as SPCE-GRAFT-Diazo-TYR (TYR-biosensor), for CC sensing.

2.4.2. Dopamine immobilization

As outlined in FIGURE 1a, the grafted SPCE was incubated with 5% of GLU solution in 50 mM PBS (pH 7.4) for 1 hour at 25°C. After that time, the surface was thoroughly rinsed and dried, followed by incubation with 2.2 mM DA in 50 mM PBS (pH 7.4) under the same conditions. After the incubation period, the modified electrode surface was rinsed with 50 mM PBS (pH 7.4) to remove any non-covalently bonded DA and then dried with a stream of air. The DA-biosensor preparation took less than 135 min.

2.4.3. Tyrosinase Enzyme Immobilization

After electrografting step (as illustrated in Figure 1b), the SPCE-GRAFT surface was covered with 25 µL of 12% $NaNO_2$ and 25 µL of 2 M HCl and allowed to react for 20 min at 4 °C. After that time, the drop was removed from the surface, rinsed and dried. Afterwards, 50 µL of tyrosinase enzyme solution (0.02 mg mL^{-1}) in 0.1 M TRIS buffer at pH 8.0 (medium to carry out the coupling reaction) were dispensed, incubating for 5 minutes at 4 °C. Once the immobilization time was up, the enzyme modified surface was rinsed with 50 mM PBS (pH 7.4) to remove the TYR enzyme that was non-covalently bonded to the surface. Finally, it was dried by means of a stream of air. The time spent in TYR-biosensor preparation does not exceed 40 min and it was kept in the cooler at 4 °C when not in use.

3. Results and Discussion

3.1. Electrografting of Gold Electrodes with 4-NBD⁺. Spectroscopic Characterization

The covalent grafting of nanometric thick organic layers onto the pretreated electrode surfaces involves the electroreduction of 4-NBD^+ in an aqueous acidic medium. The cyclic voltammograms (CVs) of the electrochemical reduction of 2 mM 4-NBD^+ solution on activated AuAT-SPE (Figure 2a) and AuBT-SPE (Figure 2b) exhibited similar electrochemical behavior in both electrodes. The first scan shows a characteristic reduction peak, associated with the formation of an aryl radical that

Preprints.org (www.preprints.org) | NOT PEER-REVIEWED | Posted: 21 February 2025 doi:10.20944/preprints202502.1766.v1

covalently bonded to the electrode surface, accompanied by the loss of N_2. The voltammograms of AuAT-SPE and AuBT-SPE exhibit cathodic peaks of -14.29 µA at 0.134 V and -22.19 µA at 0.137 V, respectively. Although the cathodic peak potentials were comparable for both gold electrodes, the higher peak current observed for AuBT-SPE suggests that its surface morphology enhances the electrochemical properties of the electrode [46].

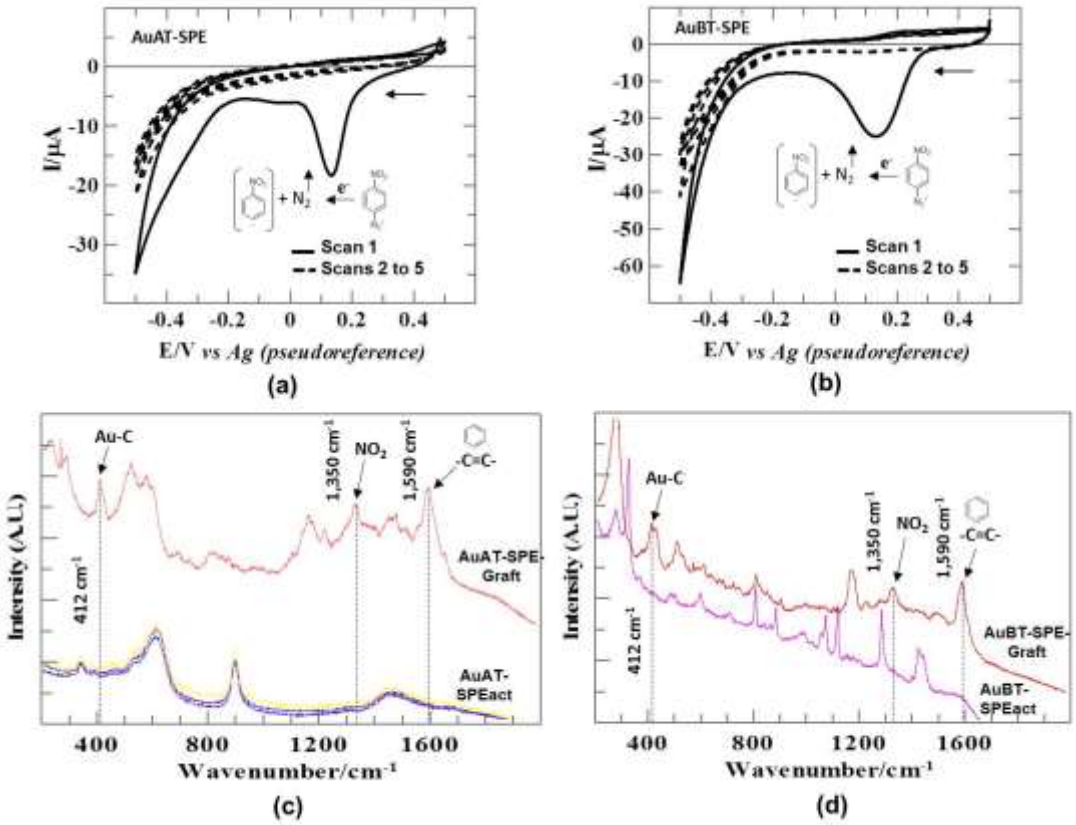

Figure 2. (a) and (b) CVs of the electrografting of 2 mM 4-NBD$^+$ in 25 mM HCl (during 5 scans at a scan rate of 100 mVs^{-1}) on an activated AuAT-SPE (a) and on an activated AuBT-SPE (b). (c) and (d) Raman-SERS spectra of AuAT-SPE (c) and AuBT-SPE (d).

To confirm the successful grafting of the nitrophenyl groups onto the gold electrodes, direct evidence was obtained using SERS spectroscopy. Figure 2c and Figure 2d depict the SERS Raman spectra for gold electrodes that were electrografted with 4-NBD$^+$. The spectra show a signal at 412 cm^{-1}, which can be attributed to the formation of an Au-C covalent bond between the gold surface and the carbon atom of the aromatic ring [47–49]. Furthermore, as shown in the figure, this signal is absent in the spectra recorded for the activated electrode (no grafting), confirming that the aryl radical was successfully bonded to the surface. In addition, the spectra exhibit the presence of signals at 1,350 cm^{-1} and 1,590 cm^{-1}, corresponding to the symmetrical stretching of the N-O bond and the stretching of the C-C bond in the aromatic ring, respectively. The absence of these bands in the spectra of bare electrode confirms the presence of aromatic molecules with nitro functional groups on the surface. This provides strong evidence that the electrode surface has been successfully modified with nitrophenyl functionalities [50].

3.2. Electrografting of Carbon Electrodes with 4-NBD$^+$. Electrochemical Characterization

Grafting onto commercial bare carbon and MWCNT modified SPCEs was performed by electrochemical reduction of 4-NBD$^+$ ions in 25 mM HCl solution on the electrode surface using CV over a wide potential window (+0.5 V to -1.0 V), which facilitates the reduction of the nitrophenyl group. Figure 3a shows the CVs of the electrografting of 2 mM 4-NBD$^+$ in 25 mM HCl on an activated

Preprints.org (www.preprints.org) | NOT PEER-REVIEWED | Posted: 21 February 2025 doi:10.20944/preprints202502.1766.v1

MWCNT-SPCE. This first scan exhibits an irreversible cathodic peak (illustrated as "(1)") with a peak potential at 0.225 V, corresponding to the formation of an aryl radical which covalently binds to the electrode surface, accompanied by the loss of N_2. Furthermore, a second wide cathodic peak (illustrated as "(2)") with two maximums is observed; the first one at -0.605 V, followed by the other at -0.720 V, which can be assigned to the electrochemical reduction of the nitrophenyl group. This process results in the formation of an aminophenyl group through a two-step reduction process with overall 6 e^- and 6 H^+ exchange, leaving the electrode surface functionalized to nanometric scale with arylamine functionalities [51]. The anodic scan (illustrated as "(3)") shows a peak at 0.180 V which can be associated with the oxidation of the aminophenyl to hydroxyaminophenyl groups [52–54]. The narrow peak observed close to 0.0 V is attributed to the carbonyl groups generated on carbon surface during the acidic electrochemical treatment (activation step).

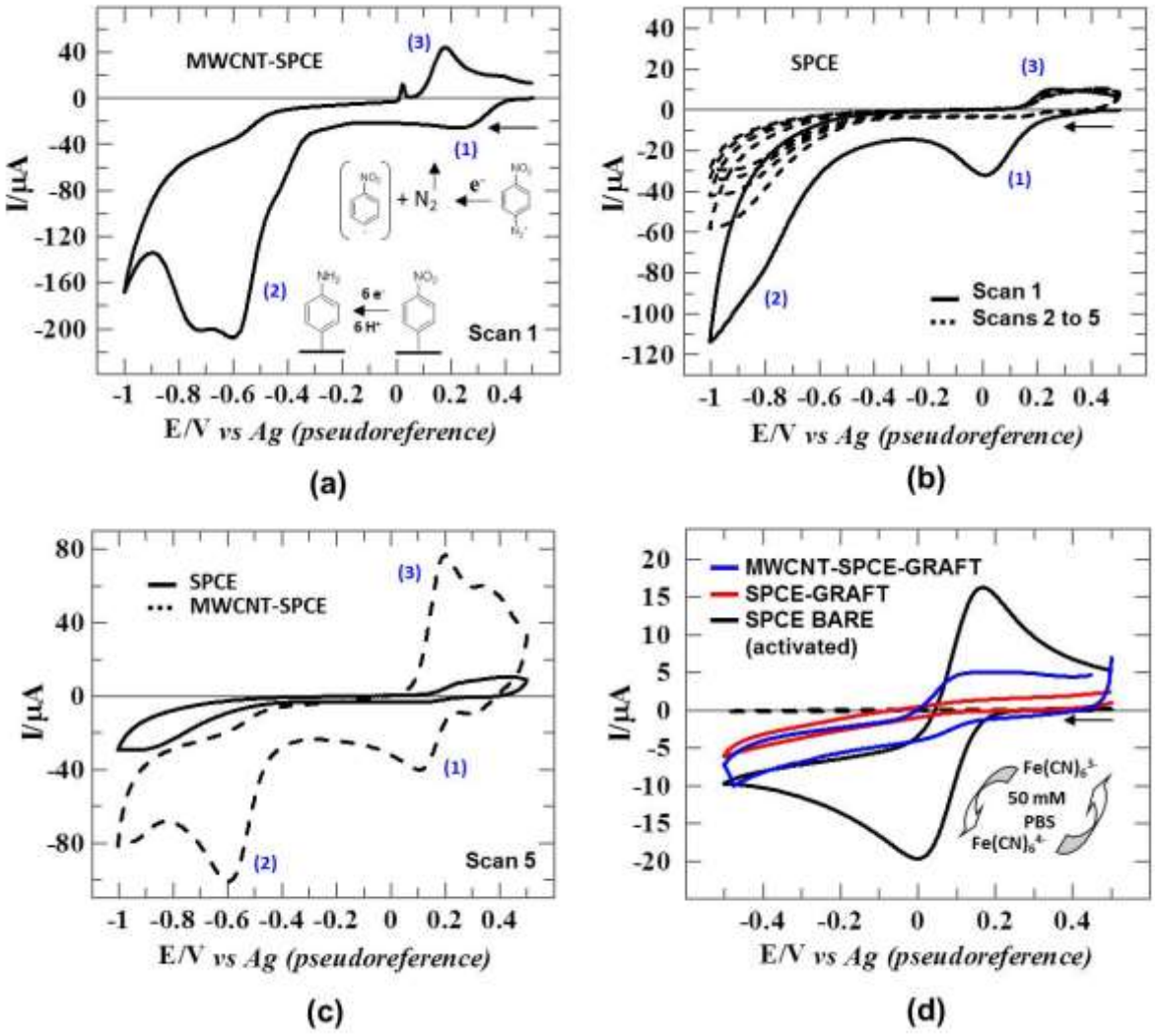

Figure 3. (a) and (b) CVs of the electrografting of 2 mM 4-NBD^+ in 25 mM HCl on activated MWCNT-SPCE (a) and on activated SPCE during 5 cycles (b). (c) Detail of 5th scan on SPCE and MWCNT-SPCE. (d) CVs of 1 mM $Fe(CN)_6^{3-}$ in 50 mM PBS (pH 7.4) on BARE SPCE (black line), SPCE-GRAFT (red line) and MWCNT-SPCE-GRAFT (blue line). Scan rate: 100 mVs^{-1}.

Figure 3b and Figure 3c show the CVs of the electrografting of 2 mM 4-NBD^+ in 25 mM HCl on an activated SPCE during 5 scans and the detail of the 5th scan on both electrodes, SPCE and MWCNT-SPCE, respectively. The first scan (depicted as black line in Figure 3b) shows the irreversible cathodic peak "(1)" and the second cathodic wave "(2)" at more negative potentials (0.006 V and -0.820V, respectively) with lower peak currents when is compared to MWCNT-SPCE (Figure 3a),

Preprints.org (www.preprints.org) | NOT PEER-REVIEWED | Posted: 21 February 2025 doi:10.20944/preprints202502.1766.v1

demonstrating the high catalytic effect of the MWCNT modifier on the electrochemical reduction processes of 4-NBD$^+$. The cathodic peaks were completely inhibited in the subsequent scans (2nd to 5th, illustrated as dashed-lines in Figure 3b), confirming the formation of a layer with blocking properties that inhibit the electronic transfer between the solution and the surface [27,55]. This inhibition is not complete on MWCNT-SPCE as can be seen in its CV illustrated in Figure 3c (dashed-line).

The electrochemical properties of SPCE-GRAFT with aminophenyl functionalities on the surface were investigated by CV in the presence of 1 mM $K_3Fe(CN)_6$ as an electroactive redox system or redox probe. Figure 3d shows the CVs of 1 mM $Fe(CN)_6^{3-}$ in an aqueous solution containing 50 mM PBS (pH 7.4), before and after the electrochemical reduction of the 4-NBD$^+$ on activated SPCE and on MWCNT-SPCE. The electrochemical response of the redox probe on bare activated SPCE (illustrated as a black line) exhibited a cathodic peak of -16.62 μA at 0.007 V and the corresponding anodic peak of 17.13 μA at 0.168V. This corresponds to the transformation of $Fe(CN)_6^{3-}$ to $Fe(CN)_6^{4-}$ and vice-versa through a one-electron process [56]. The response of the redox probe on bare activated SPCE displayed a quasi-reversible system with a peak-to-peak separation (ΔE) of 161 mV, which is significantly higher than the ideal 59 mV value, and the ratio between the current peaks was i_{pa}/i_{pc} = 1.03. After the electrografting process, the CV of the $Fe(CN)_6^{3-}$ in 50 mM PBS on SPCE-GRAFT (illustrated as a red line) showed no peaks in 50 mM PBS, indicating that a compact organic layer was formed (passivating the electrode surface) that completely blocked the electron transfer [27,54]. On the contrary, small waves and higher capacity current were observed in the CV of the redox probe on MWCNT-SPCE-GRAFT (illustrated as a blue line) that can be attributed to a poor surface covering with an organic multilayer formation that competes with dimerization and polymerization processes in the bulk solution [57].

3.3. Effect of Scan Rate on Electrografting of 4-NBD$^+$

The effect of the scan rate on the electrografting process of 4-NBD$^+$ onto SPCEs (as stated above, better option to be grafted) was evaluated by CV, monitoring the cathodic peak (peak "1" in Figure 3b) during the grafting step. CVs were recorded under the conditions of procedure (described in section 2.4.1) by varying the scan rate between 10 mVs^{-1} and 250 mVs^{-1}.

As the scan rate increased, the cathodic peak potential shifted towards more negative values, which is a characteristic profile of irreversible systems [58]. A linear relationship was observed between the cathodic peak potential and the logarithm of the scan rate, logν, according to the following Equation (1):

$$E_{pc}/V = (-0.090 \pm 0.002)\log\nu + (-0.022 \pm 0.002);\ R^2 = 0.998 \quad (1)$$

The value of αn was estimated from the slope ($2.3RT/\alpha nF$) of the above equation and the application of Laviron's equation [59–61], giving an experimental result of 0.66. Assuming α = 0.5, which is typical for irreversible processes, the number of electrons involved in the electrochemical reduction of 4-NBD$^+$ to generate the aryl radical at the SPCE was determined to be 1 e^- [62,63].

The relationship between the cathodic peak current and the scan rate showed a good linear correlation up to 100 mVs^{-1} (R^2 = 0.9990) according to the following Equation (2):

$$i_{pc}/\mu A = (153 \pm 4)\,\nu + (0.2 \pm 0.3);\ R^2 = 0.9990 \quad (2)$$

This suggests that the electrochemical process is diffusion controlled with an adsorption contribution as expected for the reason that the generated aryl radicals are grafted on the electrode surface. At higher scan rates, a decrease in peak current was observed, which can be ascribed to the formation of multilayers during the grafting step. This is a consequence of the faster generation of radicals and the progressive dimerization and polymerization processes that take place either onto surface or in the bulk solution [55].

3.4. Effect of Concentration of 4-NBD$^+$ on Surface Coverage

Preprints.org (www.preprints.org) | NOT PEER-REVIEWED | Posted: 21 February 2025 doi:10.20944/preprints202502.1766.v1

The SPE was electrografted with 4-NBD⁺ concentrations from 5 μM to 5 mM for SPCE and from 5 μM to 10 mM for AuBT-SPE (included for comparison), following the methodology described in section 2.4.1. Figure 4a shows the behavior of the cathodic peak potential (ascribed to peak "1" in Figure 3b and depicted as blue dots) as a function of the 4-NBD⁺ concentration in solution on activated SPCE (grafting step in the potential window from +0.5 V to -1.0 V). The results indicate a shift in the cathodic peak potential towards more negative values as the 4-NBD⁺ concentration increases up to 1 mM, typically for irreversible systems. Beyond this concentration, the potential shifts towards more positive values, making reduction more difficult. The cathodic peak current (represented as black dots in Figure 4a) increases with 4-NBD⁺ concentration up to 2 mM, followed by a nearly constant value up to 5 mM 4-NBD⁺. At concentrations above 3 mM, it can be assumed that the number of aryl amino functionalities on the electrode surface remains relatively constant, suggesting a saturation of the surface [63]. This fact can be corroborated by the decrease in the cathodic peak current of the redox probe, $Fe(CN)_6^{3-}$ (illustrated as red dots in Figure 4a), whose values achieve the residual current (25 mM HCl, green dots in Figure 4a) at the same time that the peak current of 4-NBD⁺ remains almost constant.

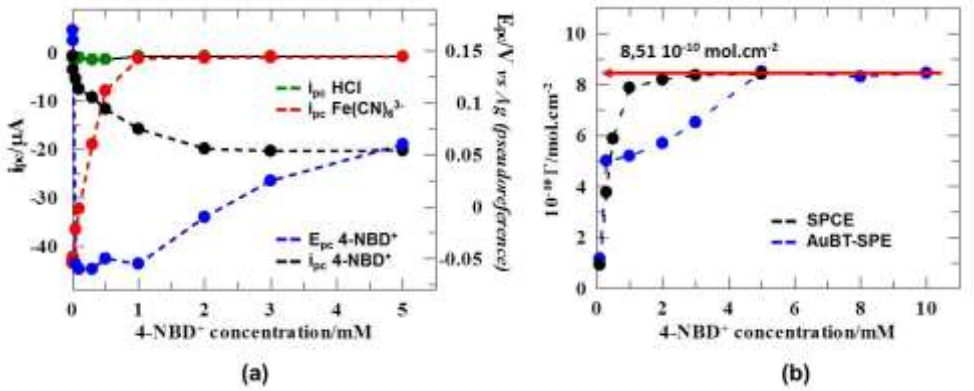

Figure 4. (a) Dependence of cathodic peak potential (blue dots) and current (black dots) of 4-NBD⁺, cathodic peak current of $Fe(CN)_6^{3-}$ (red dots) and residual current (green dots) as a function of 4-NBD⁺ concentration in 25 mM HCl on bare activated SPCE. (b) Effect of 4-NBD⁺ concentration on the surface coverage of SPCE (black dots) and AuBT-SPE (blue dots).

Figure 4b illustrates the evolution of the electrode surface coverage (Γ), calculated using Faraday's law [64], as a function of the aryldiazonium ion concentration. The SPCE surface coverage (illustrated as black dots) increases with 4-NBD⁺ concentration up to a constant value, corresponding to the maximum coverage of 8.51×10^{-10} molcm^{-2}, which is obtained at 2 mM 4-NBD⁺. The theoretical surface coverage for a compact monolayer of a 4-substituted phenyl group was calculated by Pinson and Podvorica [57], with the result being $\Gamma = 13.5\text{x}10^{-10}$ molcm^{-2}. The experimental surface coating obtained is in good agreement with the theoretical value and the small difference found can be attributed to two critical parameters: electrolysis time and grafting potential. On the one hand, the surface coating decreases as the grafting potential becomes more anodic potential [65]. On the other hand, the roughness and the real surface area (quite different from the geometric area) achieved after electrochemical treatment play an important role as well, being the values of surface coverage lower than that corresponding to the theoretical surface coverage [57]. Then, the comparison between the experimentally obtained coverage on SPCE and the theoretical value confirms that the electrografting process successfully forms a compact monolayer on the electrode surface. This is also supported by the non-observation of CV signal of the redox probe, $[Fe(CN)_6]^{3-/4-}$, illustrated as red line in Figure 3d.

However, higher 4-NBD⁺ concentrations are needed to get the maximum coating on AuBT-SPE surface (depicted as blue dots in Figure 4b). In this case, the potential window is narrower than used with SPCE, being the grafting potential more positive (grafting step in the potential window from +0.5 V to -0.5 V), achieving less surface coating for the same concentration of 2 mM 4-NBD⁺ (as stated

Preprints.org (www.preprints.org) | NOT PEER-REVIEWED | Posted: 21 February 2025 doi:10.20944/preprints202502.1766.v1

above). To achieve maximum coverage on AuBT-SPE, at least 5 mM 4-NBD$^+$ is needed, but the possibility of multilayers formation is expected, where some aryl groups can be covalently bonded together and other grafted to the surface while the remainder of the film can be the result of the adsorption [57]. All these results show that it is possible to graft effectively aryl groups from aromatic diazonium ions onto non-smooth and highly porous surfaces to produce passivate surfaces, being an excellent strategy (cheap and rapid) for the protection of many materials against environmental corrosion and other industrial applications such as electronic circuits (long-term stability of the layer).

3.5. Electrochemical Characterization of Catalytic Surface: DA-Biosensor

SPCE modified with aminophenyl groups was selected as a surface for DA immobilization via covalent bonding, using GLU as the cross-linking molecule. As illustrated in Figure 1a, the electrode surface immobilized with DA shows the characteristic CC structure in the terminal layer. The electrochemical behavior of DA-modified SPCE was investigated using CV with the redox probe $[Fe(CN)_6]^{3-/4-}$ and CC solutions.

The electrochemical response of 50 mM PBS at pH 7.4 was recorded at each step of the procedure, showing overlapped residual current in the CVs for activated SPCE BARE, SPCE-GRAFT and SPCE-GRAFT-GLU (grey dashed-line in Figure 5a). However, the voltammogram of the 50 mM PBS on SPCE-GRAFT-GLU-DA displayed an irreversible anodic signal due to oxidation of the CC groups on the electrode surface (blue line in Figure 5a), following the electrochemical reaction of Figure 5b. This fact is clear evidence of the existence of the immobilized catechol functionalities on the functionalized carbon surface. In detail, three anodic signals were observed, a pre-wave of 150 μA at 0.108 V, a second peak of 161.7 μA at 0.200 V and a third post-peak of 140 μA at 0.454V. No cathodic peak was observed in the reverse scan, indicating that the surfaces remained functionalized with terminal o-benzoquinones oriented towards the solution.

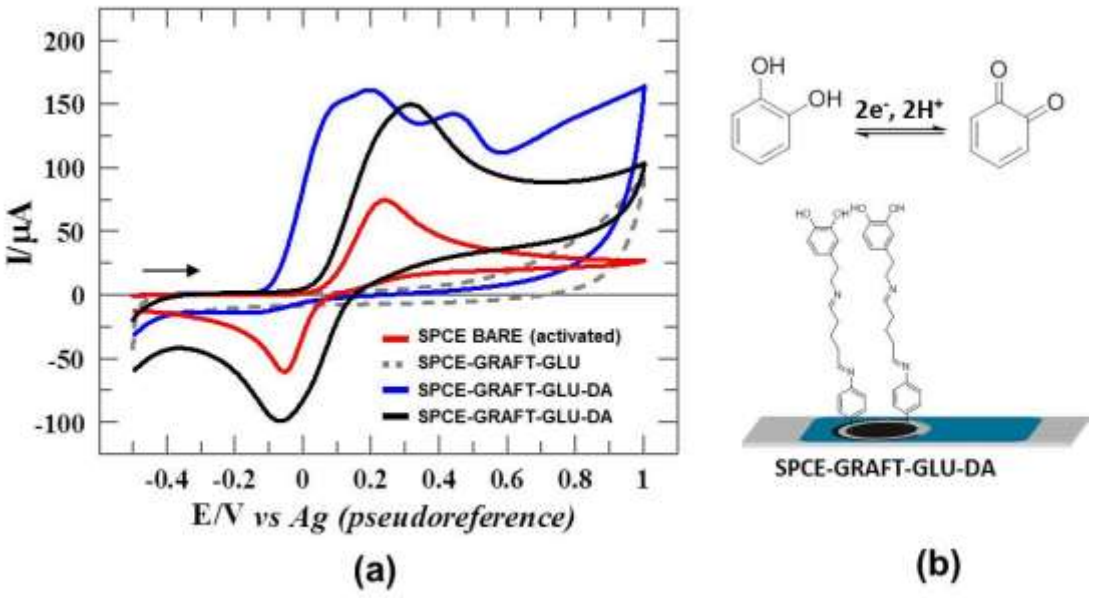

Figure 5. (a) CVs of 50 mM PBS (pH 7.4) on SPCE-GRAFT-GLU (grey dashed-line) and SPCE-GRAFT-GLU-DA (blue line). CV of 3 mM CC in 50 mM PBS on activated SPCE BARE (red line) and SPCE-GRAFT-GLU-DA (black line). Scan rate: 100 mVs^{-1}. (b) Electrochemical reaction of o-hydroxylphenyl group of CC to o-quinone either in solution or onto the modified surface.

The oxidation process of o-hydroxylphenyl group of 3 mM CC in solution to o-quinone group on activated SPCE (red line in Figure 5a and reaction in Figure 5b) can be considered as quasi-reversible, involving the exchange of 2 e$^-$ and 2 H$^+$ [66]. The CV showed an anodic peak of 73.33 μA

Preprints.org (www.preprints.org) | NOT PEER-REVIEWED | Posted: 21 February 2025 doi:10.20944/preprints202502.1766.v1

at 0.238 V and a cathodic peak of 50μA at - 0.054 V, with a ΔE of 292 mV ($E^{0\prime}$= 146 mV) and i_{pa}/i_{pc} = 1.4.

A comparative analysis between the oxidation of CC in PBS solution on activated SPCE (red line in Figure 5a) and the CC functionalities on SPCE-Graft-GLU-DA (blue line in Figure 5a) shown that the oxidation of the CC functionalities on the modified electrode surface starts to less positive values by 170 mV that the oxidation of CC in solution, accompanied by a 60% increase in the peak current. These phenomena can be ascribed to a high catalytic activity by effect of CC functionalities on the surface, confirming the formation of a covalent bond between the different self-assembled monolayers and the electrode surface, which enhances direct electron transfer.

The addition of 3 mM CC in 50 mM PBS (pH 7.4) (black line in Figure 5a) on SPCE-GRAFT-GLU-DA resulted in the characteristic voltammetric response of the CC redox process. The CV presented one anodic peak of 150 μA at 0.319 V and the corresponding cathodic peak of -90 μA at -0.070 V, giving a ΔE of 389 mV ($E^{0\prime}$= 125 mV) and the i_{pa}/i_{pc} of 1.67. As a result, the irreversibility of the process increased and the anodic and cathodic peak currents were enhanced by 2 times compared to the CC signal obtained on activated SPCE BARE (unmodified electrode), resulting in a remarkably improvement of the electrocatalytic activity towards the oxidation of CC by CC functionalities onto SPCE-GRAFT-GLU-DA modified electrode.

To investigate the electrochemical properties of the surface SPCE-GRAFT-GLU-DA, its response to an electrochemical probe, $[Fe(CN)_6]^{3-/4-}$, was evaluated by CV in all steps of the procedure (described in section 2.4.2 and depicted in Figure 1a). Figure 6 shows the voltammograms of 1 mM $Fe(CN)_6^{3-}$ in 50 mM PBS (pH 7.4) recorded in the potential window between -0.5 V and +0.5 V at 100 mVs^{-1}. The electrochemical response of the redox probe on activated SPCE BARE (black line in Figure 6a and amplified in Figure 6b), showed an anodic peak of 22.42 μA at 0.168 V and a cathodic peak of 20 μA at - 0.052 V, with a ΔE of 116 mV ($E^{0\prime}$= 58 mV) and i_{pa}/i_{pc} = 1.1, obtaining a quasi-reversible one-electron transfer process.

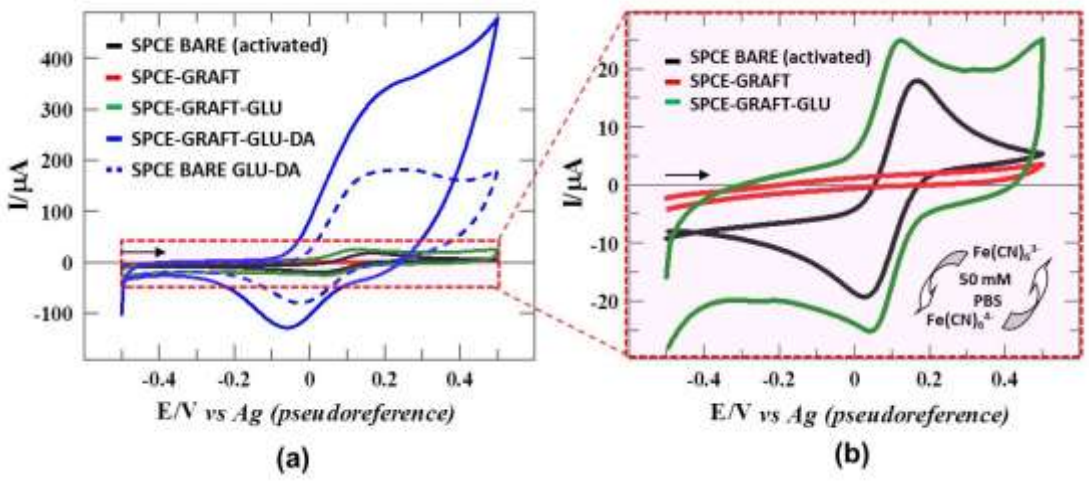

Figure 6. (a) CVs of 1 mM $Fe(CN)_6^{3-}$ in 50 mM PBS (pH 7.4) on activated SPCE BARE (black line), SPCE-GRAFT (red line), SPCE-GRAFT-GLU (green line), SPCE-GRAFT-GLU-DA (blue line) and non-grafted SPCE-GLU-DA (blue dashed-line). (b) Amplification of activated SPCE BARE, SPCE-GRAFT and SPCE-GRAFT-GLU signals. Scan rate: 100 mVs^{-1}.

As described in section 3.2, the CV of 1 mM $Fe(CN)_6^{3-}$ in 50 mM PBS on SPCE-GRAFT (red line in Figure 6a and amplified in Figure 6b) showed no discernible peaks. Therefore, the absence of a signal indicates that the conductive surface (activated SPCE) has turned into a non-conductive, confirming that the above surface was completely functionalized to nanometric scale with aminophenyl groups. The signals of $[Fe(CN)_6]^{3-/4-}$ were recovered for the SPCE-GRAFT-GLU (green line in Figure 6a and amplified in Figure 6b) to become a conductive surface again. Moreover, a shift

Preprints.org (www.preprints.org) | NOT PEER-REVIEWED | Posted: 21 February 2025 doi:10.20944/preprints202502.1766.v1

of both anodic and cathodic peaks to more negative potentials was observed, which is ascribed to the catalytic effect of the ketonic groups of GLU, oriented towards the solution (Figure 1a, step 3). The voltammogram displayed an anodic peak of 18.57 μA at 0.128 V and a corresponding cathodic peak of 18.79 μA at 0.040 V. The electrochemical process can be considered quasi-reversible as well, with a ΔE of 88 mV ($E^{0\prime}$ = 44 mV) and i_{pa}/i_{pc} = 0.99.

After the immobilization of DA on the SPCE-GRAFT-GLU surface to obtain the SPCE-GRAFT-GLU-DA (Figure 1a, step 4), this named surface exhibited excellent catalytic properties that can be associated with the presence of the terminal hydroquinone/benzoquinone couple or CC majorities at the electrode surface (blue line in Figure 6a). The CV of the 1 mM $Fe(CN)_6^{3-}$ showed an anodic peak of 316.7 μA at 0.218 V and a cathodic peak of 100 μA at -0.059 V (blue line) with ΔE = 277 mV and i_{pa}/i_{pc} = 3.17. Consequently, the electrochemical response of the redox probe on SPCE-GRAFT-GLU-DA demonstrated an increase in the irreversibility of the process, as evidenced by an increase in ΔE and i_{pa}/i_{pc} ratio. Conversely, the surface showed high catalytic activity, starting the oxidation process at more negative values by 100 mV, as well as an increase of the anodic and cathodic peak currents by a factor of 14 and 5, respectively, compared to the values obtained on activated SPCE BARE (unmodified, black line in Figure 6a and amplified in Figure 6b).

Furthermore, the redox probe response on the SPCE-GLU-DA surface was recorded, where DA immobilization was performed by direct incubation in presence of glutaraldehyde (adsorption) on an activated SPCE, thus obviating the need for an electrografting step. The CV of 1 mM $Fe(CN)_6^{3-}$ in 50 mM PBS at pH 7.4 (blue dashed-line in Figure 6a) shows an anodic peak of 100.5 μA at 0.242 V and a cathodic peak of -72.97 μA at -0.021 V, with a ΔE of 263 mV ($E^{0\prime}$ = 111 mV) and i_{pa}/i_{pc} = 1.38. After the DA immobilization, a comparison of the response obtained with the redox probe on a bare non-grafted SPCE (SPCE-GLU-DA) with that obtained on a grafted SPCE (SPCE-GRAFT-GLU-DA) revealed that the catalytic effect is lower, with a decrease in the anodic and cathodic peak currents of 68% and 27%, respectively. In addition, the signal of redox probe on SPCE-GLU-DA was lost in two days, being stable up to three months on SPCE-GRAFT-GLU-DA as the response only decreased a 7 % after that time. These results suggest that the grafting step enhances electron transfer while providing long-term stability to the biosensor, making the device robust for many applications.

3.6. DA-Biosensor for CC sensing

The high sensitivity of the SPCE-GRAFT-GLU-DA sensor enabled the construction of a calibration curve for CC in solution. In the concentration range of 0.05 mM to 10 mM, both anodic and cathodic peak currents increased proportionally with the CC concentration, exhibiting an excellent linear correlation for the anodic (Equation (3)) and cathodic (Equation (4)) peaks (Figure 7). The linear regression equations were expressed as:

$$i_{pa}/\mu A = (32.16 \pm 0.06)\,[CC]/mM + (14.5 \pm 0.2);\ R^2 = 0.9999999 \quad (3)$$

$$i_{pc}/\mu A = (-24.4 \pm 0.1)\,[CC]/mM + (-7.4 \pm 0.4);\ R^2 = 0.9999999 \quad (4)$$

Preprints.org (www.preprints.org) | NOT PEER-REVIEWED | Posted: 21 February 2025 doi:10.20944/preprints202502.1766.v1

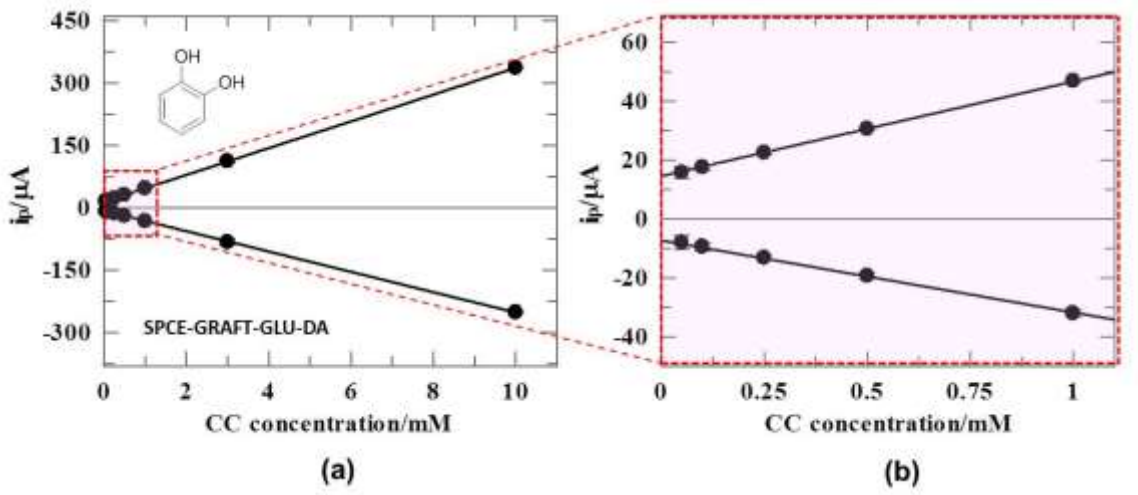

Figure 7. (a) Linear relationship between the anodic and cathodic peak currents with CC concentration on SPCE-GRAFT-GLU-DA. (b) Amplification ip *vs* [CC] for concentration from 0.05 mM to 1 mM.

The limit of detection (LOD) and limit of quantification (LOQ) were subsequently estimated through calculation using the established formulas (Equation (5) and Equation (6)):

$$LOD = \frac{3S_a}{b} \quad (5)$$

$$LOQ = \frac{10S_a}{b} \quad (6)$$

where S_a is the error of the intercept and b is the slope of the calibration curves. The LOD and LOQ for CC were determined to be 18.6 µM and 62.1 µM, respectively, with linear dynamic range (around three orders in the concentration level) from 62 µM to 10,000 µM. For two levels in the CC concentration, 250 µM and 3 mM of CC in 50 mM PBS at pH 7.4, the relative standard deviation (RSD) obtained in both was 0.8 %.

3.7. Electrochemical Characterization of TYR-Biosensor for CC sensing

The last approach presented here is the fabrication of a biosensor for detection of CC, using the $[Fe(CN)_6]^{3-/4-}$ redox probe as mediator, inferring on the catalytic effect of catechol functionalities towards the electrochemistry of $[Fe(CN)_6]^{3-/4-}$ system already observed (described in section 3.5 and shown in Figure 6). To achieve this purpose, SPCE modified with aminophenyl groups was chemically treated to generate aryl diazonium ions on the surface that were able to react by coupling reaction with the fenolic groups of TYR enzyme as indicated in section 2.4.3 and depicted in Figure 1b. The characterization of the obtained surfaces in each step was carried out with the $[Fe(CN)_6]^{3-/4-}$ system as well (as illustrated in Figure 8a). The CV of 1 mM $Fe(CN)_6^{3-}$ in 50 mM PBS at pH 7.4 on an activated SPCE BARE (black line) shows an anodic peak of 15.26 µA at 0.193 V and a cathodic peak of -15.94 µA at 0.055 V, with a ΔE of 138 mV ($E^{0'}$ = 124 mV) and i_{pa}/i_{pc} = 0.96. As expected, non-signals of redox probe were observed on SPCE-GRAFT (red line), but they were recovered on SPCE-GRAFT-Diazo-TYR (blue line). Nevertheless, the morphology and the "twisted" shape of $[Fe(CN)_6]^{3-/4-}$ voltammogram was a typical obtained on enzyme electrodes, where the peak-to-peak separation was higher by 223 mV and the peak currents lower (50%) than on activated SPCE BARE with a ratio i_{pa}/i_{pc} = 1.04. Notice that the voltammogram of the electrolyte alone on SPCE-GRAFT-Diazo-TYR (grey dashed-line) did not show any peak.

Preprints.org (www.preprints.org) | NOT PEER-REVIEWED | Posted: 21 February 2025 doi:10.20944/preprints202502.1766.v1

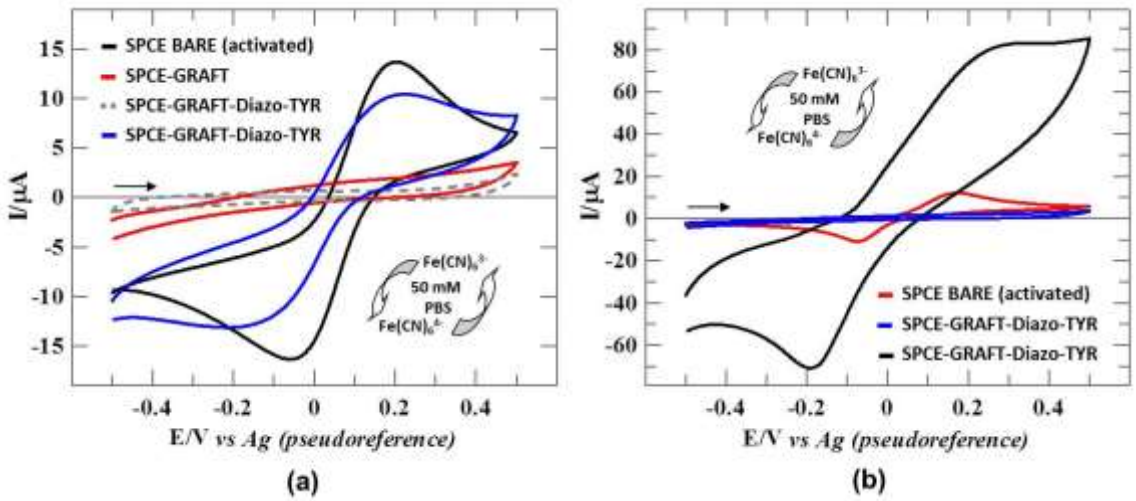

Figure 8. CVs in 50 mM PBS (pH 7.4), (a) on SPCE-GRAFT-Diazo-TYR (grey dashed-line) and in presence of 1 mM $Fe(CN)_6^{3-}$ on SPCE-GRAFT-Diazo-TYR (blue line), on activated SPCE BARE (black line) and SPCE-GRAFT (red line). (b) 200 µM CC on unmodified SPCE BARE (red line) and 1 mM $Fe(CN)_6^{3-}$ as mediator on SPCE-GRAFT-Diazo-TYR, in absence (blue line) and in presence of 200 µM CA (black line). Scan rate: 100 mVs^{-1}.

As stated above for 3 mM CC in 50 mM PBS (pH 7.4) on activated SPE BARE (red line in Figure 5a), the electrochemical behavior for 200 µM CC in same conditions was quasi-reversible as well (red line in Figure 8b), giving rise to two observable peaks that appeared at 0.169 V with a peak current of 9.77 µA and at -0.075 V with a peak current of -10.81 µA on the forward and on the reverse scans, respectively, with a ΔE of 244 mV ($E^{0\prime}$= 47 mV) and i_{pa}/i_{pc} = 0.90. In contrast, an impressive catalytic current was observed for 1 mM $Fe(CN)_6^{3-}$ on SPCE-GRAFT-Diazo-TYR in presence of 200 µM CC (black line in Figure 8b) in comparison to that obtained in absence of CC (blue line in both Figure 8a and Figure 8b), achieving an increase of the signal of about 10 times for the same CC concentration.

To obtain information about the response of the TYR-biosensor towards CC in presence of the mediator (Figure 9a), the concentration dependence of CC over the range 50 µM to 400 µM was investigated by plotting the peak current of mediator obtained by each CC concentration (illustrated as red dots in Figure 9b), exhibiting an excellent linear correlation for the anodic peak of $[Fe(CN)_6]^{3-/4-}$ system that follows the linear regression equation (Equation (7)).

$$i_{pa}/\mu A = (317 \pm 7)\,[CC]/mM + (0.1 \pm 0.5);\ R^2 = 0.9992 \qquad (7)$$

It is worth noting that the impressive sensitivity of TYR-biosensor was tenfold higher compared to the also sensitive DA-biosensor (as already mentioned), as demonstrated by the values of the slopes from linear regressions, Equation (3) and Equation (7), and shown in Figure 9b. The developed TYR-biosensor presented a LOD and LOQ of 4.5 µM and 14.9µM, respectively, with a RSD of 1.4 % for 200 µM CC in the concentration level.

Preprints.org (www.preprints.org) | NOT PEER-REVIEWED | Posted: 21 February 2025 doi:10.20944/preprints202502.1766.v1

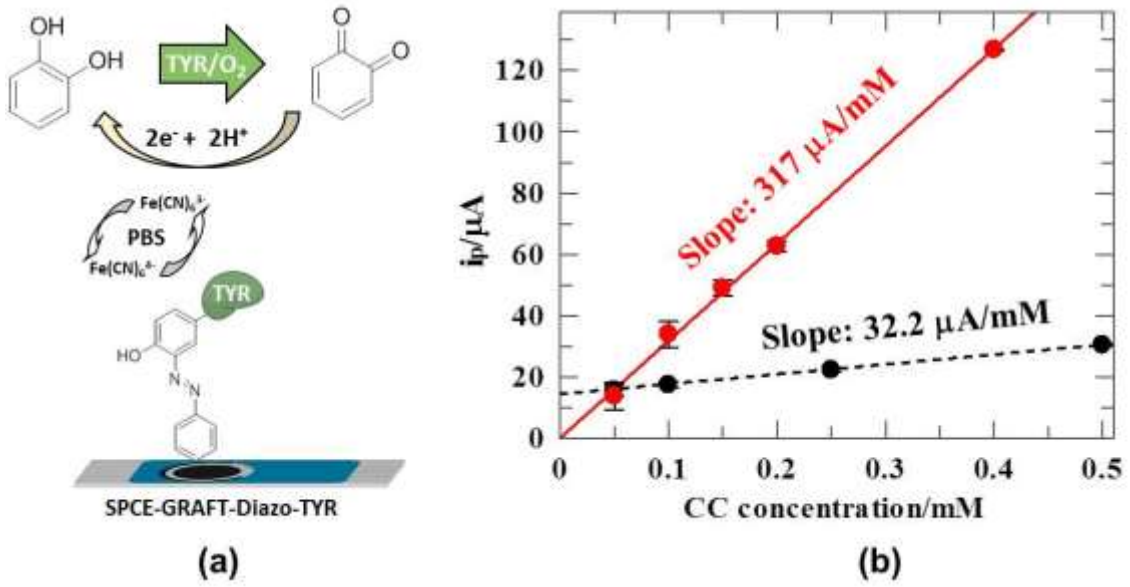

Figure 9. (a) Electrochemical detection of CC via TYR enzyme and $[Fe(CN)_6]^{3-/4-}$ mediator reactions. (b) Sensitivity (slope) comparison of CC calibration on catalytic SPCE-GRAFT-GLU-DA (black dots) (data extracted from Figure 7) and SPCE-GRAFT-Diazo-TYR surfaces (red dots).

The analytical parameters obtained from the SPCE-GRAFT-GLU-DA and SPCE-GRAFT-Diazo-TYR surfaces for CC sensing were compared to those of other (bio)sensor devices based on carbon electrodes reported in the literature (see Table 1). It is noteworthy that both (bio)sensors exhibit remarkable sensitivity, even when compared to devices employing differential pulse voltammetry (DPV) or square wave voltammetry (SWV), techniques that are recognized for their higher sensitivity than CV. A comparison of the (bio)sensors performance with other sensors utilising CV reveals LOD similar or lower, thereby demonstrating its enhanced performance. Moreover, the SPCE-GRAFT-GLU-DA (bio)sensor developed in this study exhibits a broader dynamic range, spanning three orders of magnitude in concentration that none reaches. This expanded linear range for DA-biosensor and the impressive sensitivity for TYR-biosensor, coupled with the short manufacturing time for fabrication required and the low-priced reagents used, highlights the potential of both (bio)sensors described here for practical applications in the detection of CC without the need for complex nanostructure modifications.

Table 1. Analytical performance comparison of different unmodified and modified carbon electrodes for CC sensing.

Electrode*	Technique**	LDR*** (µM)	LOD (µM)	Sensitivity (µA/mM)	Ref.
SPCE/GNPs	DPV	23 – 200	6.9	150	[67]
SPCE	SWV	20 – 220	5.9	31.0	[68]
GCE/Fe3O4-TiO2	CV	150 – 500	45	5.6	[69]
GCE/MWCNT/NiO	DPV	10 – 400	2.5	196	[70]
GCE/GR/CdTe-QDs	DPV	80 – 1,000	18.3	6.4	[71]
GCE/PTA	DPV	26 – 500	7.8	120	[72]
GCE/RGO-MWNTs	DPV	6 – 540	1.8	70	[73]
SPCE/Cu-CMCS2	CA	7.3 – 40	7.3	10.0	[33]
SPCE/TYR	CA	29 – 40	29	3.3	[33]

Preprints.org (www.preprints.org) | NOT PEER-REVIEWED | Posted: 21 February 2025 doi:10.20944/preprints202502.1766.v1

GCE/CMS-g-PANI@MWCNTs/TYR	DPV	83 – 100	25	78.5	[38]
SPCE/MNP/MWCNTs/TYR	DPV	10 – 80	7.6	4.8	[74]
GCE-DHP/AuNPs/TYR	Amp.	2.5 – 95	0.7	115	[31]
GCE-MLN/AO/TYR	Amp.	1.7 – 80	0.5	31.5	[75]
GCE/PS-ND/TYR	DPV	5 – 740	0.9	23.0	[32]
GCE/ZnO/TYR/Nafion	Amp.	13 – 400	6	2.14	[76]
CBPE/GLU/TYR	Amp.	0.05 – 8.5	0.015	460	[77]
CGGE-PET/MWCNT/TYR	CA	0.5 – 50	0.3	231	[78]
GCE/MWCNT-IL-TYR	LSV	4.9 – 1,100	0.6	32.8	[79]
SPCE/CB4/TYR	CV	6.3 – 100	1.9	130	[80]
SPCE/BSA-GLU/TYR	DPV	19 – 103	5.6	6.2	[36]
GCE/pTN-GLU/TYR	CV	20 – 300	6.0	5.04	[81]
SPCE-GRAFT-GLU-DA	**CV**	**62 – 10,000**	**18.6**	**32.2**	**This work**
SPCE-GRAFT-Diazo-TYR	**CV**	**14.9 – 400**	**4.5**	**317**	**This work**

*Acridine orange (AO); bovine serum albumin (BSA); 1-butyl-3-methylimidazolium chloride (ionic liquid= IL); cadmium telluride quantum dots (CdTe-QDs); carbon black ink (CB4); carbon black paste electrode (CBPE); carbon nanodiamonds (NDs); carboxymethyl starch (CMS); chitosan biopolymer, graphite powder and glycerol mixture electrode CGGE); enzyme-less Cu-Cubic mesoporous carbon stage 2 (Cu-CMCS2); dihexadecylphosphate (DHP); glassy carbon electrode (GCE); glutaraldehyde (GLU); graphene nanoplatelets (GNPs); magnetic nanoparticles (MNP); multi-walled carbon nanotubes (MWCNT); natural molybdenite (MLN); polyaniline (PANI); polyethylene terephthalate (PET); poly-thionine (pTN); poly-3-thiophenemalonic acid (PTA); potato starch (PS); reduced graphene oxide (RGO); screen-printed carbon electrode (SPCE); tyrosinase (TYR).

**Amperometry (Amp.); chronoamperometry (CA); cyclic voltammetry (CV); differential pulse voltammetry (DPV); linear sweep voltammetry (LSV); square-wave voltammetry (SWV).

***Linear Dynamic Range was estimated from the upper and the lower concentration (LOD) given by the authors, calculating the LOQ as LOD by 3.33 that will be the minimum concentration to be determined with an acceptable repeatability and trueness, being therefore the lower limit in the linear dynamic range.

5. Conclusions

The electrochemical reduction of aryldiazonium ion represents a rapid, simple and versatile methodology for the surface grafting of organic layers on any type of material. In addition, the rich chemistry of these compounds applied to achieve the immobilization of biomolecules by covalent bond is impressive. This work demonstrates that SPE functionalized with 4-NBD$^+$ ion provides robust and compact platforms capable of anchoring delicate biological components, such as DA or TYR, or serving as a protective insulating layer to prevent corrosion by passivation of the electrode surface. Through the optimization of critical parameters, including scan rate, potential window and 4-NBD$^+$ concentration, the formation of a thin organic layer on a rough and highly porous surface with the highest surface coverage was achieved. Specifically, the electrochemical reduction of a 2 mM 4-NBD$^+$ solution in 25 mM HCl resulted in the optimal surface coverage when 5 cyclic scans were applied in the potential window of +0.5 V to -1.0 V at 100 mVs^{-1}, achieving the functionalization to nanometric scale with aminophenyl groups oriented towards the bulk solution.

Preprints.org (www.preprints.org) | NOT PEER-REVIEWED | Posted: 21 February 2025 doi:10.20944/preprints202502.1766.v1

Briefly, the SPCE-GRAFT-GLU-DA biosensor is stable, robust, simple and low cost. It exhibited noteworthy catalytic activity towards $[Fe(CN)_6]^{3-/4-}$, a redox mediator commonly involved in various enzymatic reactions. The proposed sensor produced analytical signals 14 times higher than those observed on unmodified surfaces under near-physiological conditions (25°C, 0.05 M ionic strength, and pH 7.4), highlighting the sensor's adaptability to biochemical environments. The enhanced electron transfer kinetics and stability of the modified surface underscore its potential for diverse electrochemical applications. Furthermore, when utilized for the detection of CC, the SPCE-GRAFT-GLU-DA sensor demonstrated a limit of detection of 4.6 μM and a linear range extending three concentration units.

Additionally, the immobilization of TYR on a grafted surface via *in situ* diazotation followed by a coupling reaction was also conducted, giving rise to the SPCE-GRAFT-Diazo-TYR biosensor. This TYR-biosensor, in addition to being highly selective due to the presence of the enzyme, also demonstrated high sensitivity. Specifically, the observed catalytic effect in $[Fe(CN)_6]^{3-/4-}$ mediator detection was 10 times higher than the already sensitive SPCE-GRAFT-GLU-DA biosensor. Furthermore, immobilization by covalent bond confers additional stability to the (bio)sensor, thus counteracting the problem of the low stability of the enzymes and ensuring the reproducibility of the results. When applying the SPCE-GRAFT-Diazo-TYR biosensor to the determination of CC, a narrower linear range was obtained than with the SPCE-GRAFT-GLU-DA. In contrast, the comparison of the slopes obtained allows inferring that the enzymatic biosensor is 10 times more sensitive. All these results suggest an interesting new line of research to explore the electrochemical response of the (bio)sensor to enzymatic reaction products such as hydrogen peroxide and NADH or the use of $[Fe(CN)_6]^{3-/4-}$ as mediator in many other enzymatic reactions.

Therefore, the proposed (bio)sensors are very competitive with those that appear in the bibliography and they can also be ideal devices for applications in direct analyte detection and enzymatic assays. Their long-term stability (more than three months for DA-biosensor and one month for TYR-biosensor) and their robust performance under physiological conditions suggest their potential for integration into portable sensing platforms for *in-situ* diagnostics and real-time monitoring. Although all these results are promising, further research is required to quantify catechol in real and complex samples as environmental ones, using more sensitive techniques than CV and considering matrix effects and potential interferences as well.

6. Patents

This research is part of the studies begun in 2007 that led to the application for a Patent in 2010, with title "Catalytic Surface", filed on April 5, 2011 and granted by Spanish Patent and Trademark Office (OEPM) with registration number: ES 2 389 936 B2 on January 17, 2014. (https://consultas2.oepm.es/pdf//ES/0000/000/02/38/99/ES-2389936_B2.pdf).

Author Contributions: Conceptualization, J.M. G-C. and E. G-R.; methodology, E. G-R.; validation, E. G-R.; formal analysis, J.M. G-C. and S. C-P.; investigation, J.M. G-C. and E. G-R.; resources, J.M. G-C., S. C-P. and E. G-R.; data curation, J.M. G-C. and S. C-P.; writing—original draft preparation, J.M. G-C. and E. G-R.; writing—review and editing, J.M. C-G, S. C-P. and E. G-R.; visualization, J.M. C-G. and E. G-R; supervision, E. G-R.; project administration, E. G-R.; funding acquisition, E. G-R. All authors have read and agreed to the published version of the manuscript..

Funding: This research was funded by University of Vigo, grant number 07V1A13 and the Protection of Research Results by PCT Patent Extension. The APC was funded by Universidade de Vigo/CISUG/CRUE and Applied Science journal (MDPI).

Institutional Review Board Statement: Not applicable

Informed Consent Statement: Not applicable

Data Availability Statement: Data are contained within the article.

Preprints.org (www.preprints.org) | NOT PEER-REVIEWED | Posted: 21 February 2025 doi:10.20944/preprints202502.1766.v1

Acknowledgments: The authors would like to thank Isabel Pastoriza-Santos, Jorge Pérez-Juste and Vanesa López-Puente for their commitment to the characterization of surfaces through Raman spectroscopy. The authors are grateful to Applied Sciences journal Editorial Office for their kindness and support in providing to publish this work free-of-charge.

Conflicts of Interest: The authors declare no conflicts of interest.

Abbreviations

The following abbreviations are used in this manuscript:

4-NBD$^+$	4-Nitrobenzenediazonium ions
Amp	Amperometry
AO	Acridine Orange
AuAT-SPE	Screen-Printed Gold Electrode (High temperature cured ink)
AuBT-SPE	Screen-Printed Gold Electrode (Low temperature cured ink)
AuNPs	Gold nanoparticles
BSA	Bovine Serum Albumin
BDD	Boron-Doped Diamond
CC	Catechol
CA	Chronoamperometry
CB4	Carbon Black Ink
CBPE	Carbon Black Paste Electrode
CdTe-QDs	Cadmium Telluride Quantum Dots
CGGE	Chitosan Biopolymer, Graphite Powder and Glycerol Mixture Electrode
CMS	Carboxymethyl Starch
Cu-CMCS2	Enzyme-less-Cubic Mesoporous Carbon Stage 2 (Tyrosinase-mimicking)
CV	Cyclic Voltammetry/Cyclic voltammogram
CVs	Cyclic voltammograms
DA	Dopamine
Diazo	Surface modified by diazotization reaction
DHP	Dihexadecylphosphate
DPV	Differential Pulse Voltammetry
E_{pa}	Anodic peak potential
E_{pc}	Cathodic peak potential
GCE	Glassy Carbon Electrode
GLU	Glutaraldehyde
GNPs	Graphene Nanoplatelets
GR	Graphene
GRAFT	Surface modified with aminophenyl groups
IL	Ionic Liquid
i_{pa}	Anodic peak current
i_{pc}	Cathodic peak current
ITO	Indium Tin Oxide
LDR	Linear Dynamic Range

Preprints.org (www.preprints.org) | NOT PEER-REVIEWED | Posted: 21 February 2025 doi:10.20944/preprints202502.1766.v1

LOD	Limit of Detection
LOQ	Limit of Quantification
LSV	Linear Sweep Voltammetry
MLN	Natural Molybdenite
MNP	Magnetic Nanoparticles
MWCNTs	Multiwalled Carbon Nanotubes
NDs	Carbon Nanodiamonds
PANI	Polyaniline
PBS	Phosphate-Buffered Solution
PEDOT	Poly(3,4-ethylenedioxythiophene)
PET	Polyethylene Terephthalate
PTA	Poly-3-Thiophenemalonic Acid
PS	Potato Starch
pTN	Poly-Thionine
RGO	Reduced Graphene Oxide
RSD	Relative standard deviation
SERS	Surface-Enhanced Raman Spectroscopy
SPE	Screen-Printed Electrode
SPCE	Screen-Printed Carbon Electrode
SWV	Square Wave Voltammetry
TRIS	2-Amino-2-(hidroxymethyl)-1,3-propanediol
TYR	Tyrosinase

References

1. Hetemi, D.; Noël, V.; Pinson, J. Grafting of Diazonium Salts on Surfaces: Application to Biosensors. *Biosensors* **2020**, *10*, 4, doi:10.3390/bios10010004.
2. Chehimi, M.M. *Aryl Diazonium Salts: New Coupling Agents in Polymer and Surface Science*; 1st ed.; Wiley, 2012; ISBN 978-3-527-32998-4.
3. Toupin, M.; Bélanger, D. Thermal Stability Study of Aryl Modified Carbon Black by in Situ Generated Diazonium Salt. *J. Phys. Chem. C* **2007**, *111*, 5394–5401, doi:10.1021/jp066868e.
4. Liu, G.; Böcking, T.; Gooding, J.J. Diazonium Salts: Stable Monolayers on Gold Electrodes for Sensing Applications. *Journal of Electroanalytical Chemistry* **2007**, *600*, 335–344, doi:10.1016/j.jelechem.2006.09.012.
5. Haque, A.-M.J.; Kim, K. Reusable Bio-Functionalized Surfaces Based on Electrochemical Desorption of Benzenediazonium-Grafted Organic Layers. *Chem. Commun.* **2011**, *47*, 6855, doi:10.1039/c1cc11866h.
6. Randriamahazaka, H.; Ghilane, J. Electrografting and Controlled Surface Functionalization of Carbon Based Surfaces for Electroanalysis. *Electroanalysis* **2016**, *28*, 13–26, doi:10.1002/elan.201500527.
7. Matrab, T.; Chancolon, J.; L'hermite, M.M.; Rouzaud, J.-N.; Deniau, G.; Boudou, J.-P.; Chehimi, M.M.; Delamar, M. Atom Transfer Radical Polymerization (ATRP) Initiated by Aryl Diazonium Salts: A New Route for Surface Modification of Multiwalled Carbon Nanotubes by Tethered Polymer Chains. *Colloids and Surfaces A: Physicochemical and Engineering Aspects* **2006**, *287*, 217–221, doi:10.1016/j.colsurfa.2006.05.028.
8. Matyjaszewski, K.; Xia, J. Atom Transfer Radical Polymerization. *Chem. Rev.* **2001**, *101*, 2921–2990, doi:10.1021/cr940534g.
9. Iruthayaraj, J.; Chernyy, S.; Lillethorup, M.; Ceccato, M.; Røn, T.; Hinge, M.; Kingshott, P.; Besenbacher, F.; Pedersen, S.U.; Daasbjerg, K. On Surface-Initiated Atom Transfer Radical Polymerization Using Diazonium Chemistry To Introduce the Initiator Layer. *Langmuir* **2011**, *27*, 1070–1078, doi:10.1021/la104125n.

Preprints.org (www.preprints.org) | NOT PEER-REVIEWED | Posted: 21 February 2025 doi:10.20944/preprints202502.1766.v1

10. Laforgue, A.; Addou, T.; Bélanger, D. Characterization of the Deposition of Organic Molecules at the Surface of Gold by the Electrochemical Reduction of Aryldiazonium Cations. *Langmuir* **2005**, *21*, 6855–6865, doi:10.1021/la047369c.
11. Lee, L.; Brooksby, P.A.; Hapiot, P.; Downard, A.J. Electrografting of 4-Nitrobenzenediazonium Ion at Carbon Electrodes: Catalyzed and Uncatalyzed Reduction Processes. *Langmuir* **2016**, *32*, 468–476, doi:10.1021/acs.langmuir.5b03233.
12. Pilan, L. Tailoring the Performance of Electrochemical Biosensors Based on Carbon Nanomaterials via Aryldiazonium Electrografting. *Bioelectrochemistry* **2021**, *138*, 107697, doi:10.1016/j.bioelechem.2020.107697.
13. Combellas, C.; Jiang, D.; Kanoufi, F.; Pinson, J.; Podvorica, F.I. Steric Effects in the Reaction of Aryl Radicals on Surfaces. *Langmuir* **2009**, *25*, 286–293, doi:10.1021/la8025792.
14. Greenwood, J.; Phan, T.H.; Fujita, Y.; Li, Z.; Ivasenko, O.; Vanderlinden, W.; Van Gorp, H.; Frederickx, W.; Lu, G.; Tahara, K.; et al. Covalent Modification of Graphene and Graphite Using Diazonium Chemistry: Tunable Grafting and Nanomanipulation. *ACS Nano* **2015**, *9*, 5520–5535, doi:10.1021/acsnano.5b01580.
15. Georgakilas, V.; Otyepka, M.; Bourlinos, A.B.; Chandra, V.; Kim, N.; Kemp, K.C.; Hobza, P.; Zboril, R.; Kim, K.S. Functionalization of Graphene: Covalent and Non-Covalent Approaches, Derivatives and Applications. *Chem. Rev.* **2012**, *112*, 6156–6214, doi:10.1021/cr3000412.
16. Wang, J.; Firestone, M.A.; Auciello, O.; Carlisle, J.A. Surface Functionalization of Ultrananocrystalline Diamond Films by Electrochemical Reduction of Aryldiazonium Salts. *Langmuir* **2004**, *20*, 11450–11456, doi:10.1021/la048740z.
17. Haghshenas, E.; Madrakian, T.; Afkhami, A.; Saify Nabiabad, H. An Electrochemical Ceruloplasmin Aptasensor Using a Glassy Carbon Electrode Modified by Diazonium-Functionalized Multiwalled Carbon Nanotubes. *J IRAN CHEM SOC* **2019**, *16*, 593–602, doi:10.1007/s13738-018-1533-6.
18. Kang, S.J.; Kim, S.; Lee, K.; Shin, I.-S.; Kim, Y.-R. Tunable Electrochemical Grafting of Diazonium for Highly Sensitive Impedimetric DNA Sensor. *J. Electrochem. Soc.* **2020**, *167*, 087504, doi:10.1149/1945-7111/ab8ce8.
19. Mooste, M.; Kibena, E.; Matisen, L.; Tammeveski, K. Blocking Properties of Nickel Electrodes Modified with Aryldiazonium Compounds. *International Journal of Electrochemical Science* **2015**, *10*, 3803–3819, doi:10.1016/S1452-3981(23)06581-1.
20. Combellas, C.; Delamar, M.; Kanoufi, F.; Pinson, J.; Podvorica, F.I. Spontaneous Grafting of Iron Surfaces by Reduction of Aryldiazonium Salts in Acidic or Neutral Aqueous Solution. Application to the Protection of Iron against Corrosion. *Chem. Mater.* **2005**, *17*, 3968–3975, doi:10.1021/cm050339q.
21. İsbir-Turan, A.A.; Üstündağ, Z.; Solak, A.O.; Kılıç, E.; Avseven, A. Electrochemical and Spectroscopic Characterization of a Benzo[c]Cinnoline Electrografted Platinum Surface. *Thin Solid Films* **2009**, *517*, 2871–2877, doi:10.1016/j.tsf.2008.10.073.
22. Ullien, D.; Thüne, P.C.; Jager, W.F.; Sudhölter, E.J.R.; De Smet, L.C.P.M. Controlled Amino-Functionalization by Electrochemical Reduction of Bromo and Nitro Azobenzene Layers Bound to Si(111) Surfaces. *Phys. Chem. Chem. Phys.* **2014**, *16*, 19258–19265, doi:10.1039/C4CP02464H.
23. Yates, N.D.; Dowsett, M.R.; Bentley, P.; Dickenson-Fogg, J.A.; Pratt, A.; Blanford, C.F.; Fascione, M.A.; Parkin, A. Aldehyde-Mediated Protein-to-Surface Tethering via Controlled Diazonium Electrode Functionalization Using Protected Hydroxylamines. *Langmuir* **2020**, *36*, 5654–5664, doi:10.1021/acs.langmuir.9b01254.
24. Richard, W.; Evrard, D.; Gros, P. A Novel Electrochemical Sensor Based on a Mixed Diazonium/PEDOT Surface Functionalization for the Simultaneous Assay of Ascorbic and Uric Acids. Towards an Improvement in Amperometric Response Stability. *Electroanalysis* **2014**, *26*, 1390–1399, doi:10.1002/elan.201300632.
25. Lo, M.; Diaw, A.K.D.; Gningue-Sall, D.; Aaron, J.-J.; Oturan, M.A.; Chehimi, M.M. Tracking Metal Ions with Polypyrrole Thin Films Adhesively Bonded to Diazonium-Modified Flexible ITO Electrodes. *Environ Sci Pollut Res* **2018**, *25*, 20012–20022, doi:10.1007/s11356-018-2140-x.
26. Hayat, A.; Barthelmebs, L.; Sassolas, A.; Marty, J.-L. An Electrochemical Immunosensor Based on Covalent Immobilization of Okadaic Acid onto Screen Printed Carbon Electrode via Diazotization-Coupling Reaction. *Talanta* **2011**, *85*, 513–518, doi:10.1016/j.talanta.2011.04.034.

Preprints.org (www.preprints.org) | NOT PEER-REVIEWED | Posted: 21 February 2025 doi:10.20944/preprints202502.1766.v1

27. Revenga-Parra, M.; García-Mendiola, T.; González-Costas, J.; González-Romero, E.; Marín, A.G.; Pau, J.L.; Pariente, F.; Lorenzo, E. Simple Diazonium Chemistry to Develop Specific Gene Sensing Platforms. *Analytica Chimica Acta* **2014**, *813*, 41–47, doi:10.1016/j.aca.2014.01.026.
28. Bounegru, A.V.; Apetrei, C. Tyrosinase Immobilization Strategies for the Development of Electrochemical Biosensors—A Review. *Nanomaterials* **2023**, *13*, 760, doi:10.3390/nano13040760.
29. Raymundo-Pereira, P.A.; Silva, T.A.; Caetano, F.R.; Ribovski, L.; Zapp, E.; Brondani, D.; Bergamini, M.F.; Marcolino, L.H.; Banks, C.E.; Oliveira, O.N.; et al. Polyphenol Oxidase-Based Electrochemical Biosensors: A Review. *Analytica Chimica Acta* **2020**, *1139*, 198–221, doi:10.1016/j.aca.2020.07.055.
30. Vlamidis, Y.; Gualandi, I.; Tonelli, D. Amperometric Biosensors Based on Reduced GO and MWCNTs Composite for Polyphenols Detection in Fruit Juices. *Journal of Electroanalytical Chemistry* **2017**, *799*, 285–292, doi:10.1016/j.jelechem.2017.06.012.
31. Campanhã Vicentini, F.; Garcia, L.L.C.; Figueiredo-Filho, L.C.S.; Janegitz, B.C.; Fatibello-Filho, O. A Biosensor Based on Gold Nanoparticles, Dihexadecylphosphate, and Tyrosinase for the Determination of Catechol in Natural Water. *Enzyme and Microbial Technology* **2016**, *84*, 17–23, doi:10.1016/j.enzmictec.2015.12.004.
32. Camargo, J.R.; Baccarin, M.; Raymundo-Pereira, P.A.; Campos, A.M.; Oliveira, G.G.; Fatibello-Filho, O.; Oliveira, O.N.; Janegitz, B.C. Electrochemical Biosensor Made with Tyrosinase Immobilized in a Matrix of Nanodiamonds and Potato Starch for Detecting Phenolic Compounds. *Analytica Chimica Acta* **2018**, *1034*, 137–143, doi:10.1016/j.aca.2018.06.001.
33. Jayaraman, S.; Rajarathinam, T.; Chakravarthi Nagarajan, D.; Kandasamy, P.; Jeon, S.; Kim, C.-S.; Won Hong, S.; Paik, H.; Chang, S.-C. A Smartphone-Based Tunable Tyrosinase Functional Mimic Modulated Portable Amperometric Sensor for the Rapid and Real-Time Monitoring of Catechol. *Chemical Engineering Journal* **2024**, *497*, 154811, doi:10.1016/j.cej.2024.154811.
34. Baluta, S.; Meloni, F.; Halicka, K.; Szyszka, A.; Zucca, A.; Pilo, M.I.; Cabaj, J. Differential Pulse Voltammetry and Chronoamperometry as Analytical Tools for Epinephrine Detection Using a Tyrosinase-Based Electrochemical Biosensor. *RSC Adv.* **2022**, *12*, 25342–25353, doi:10.1039/D2RA04045J.
35. Nurul Karim, Md.; Lee, H.J. Amperometric Phenol Biosensor Based on Covalent Immobilization of Tyrosinase on Au Nanoparticle Modified Screen Printed Carbon Electrodes. *Talanta* **2013**, *116*, 991–996, doi:10.1016/j.talanta.2013.08.003.
36. Rita Montereali, M.; Vastarella, W.; Della Seta, L.; Pilloton, R. Tyrosinase Biosensor Based on Modified Screen Printed Electrodes: Measurements of Total Phenol Content. *International Journal of Environmental Analytical Chemistry* **2005**, *85*, 795–806, doi:10.1080/03067310500149775.
37. Vulcano, F.; Kovtun, A.; Bettini, C.; Xia, Z.; Liscio, A.; Terzi, F.; Heras, A.; Colina, A.; Zanfrognini, B.; Melucci, M.; et al. Dopamine-Functionalized Graphene Oxide as a High-Performance Material for Biosensing. *2D Mater.* **2020**, *7*, 024007, doi:10.1088/2053-1583/ab734f.
38. Mollamohammadi, F.; Faridnouri, H.; Zare, E.N. Electrochemical Biosensing of L-DOPA Using Tyrosinase Immobilized on Carboxymethyl Starch-Graft-Polyaniline@MWCNTs Nanocomposite. *Biosensors* **2023**, *13*, 562, doi:10.3390/bios13050562.
39. Goodarzi, M.; Tavakoli, H.; Khalaj, M.A.; Tavakoli, H. A Novel Approach to Tyrosinase-Based Biosensors: Electrode Reactions and Biological Measurement. *Biosensors and Bioelectronics: X* **2024**, *21*, 100550, doi:10.1016/j.biosx.2024.100550.
40. Hosseinzadeh, L.; Khoshroo, A.; Adib, K.; Rahimi-Nasrabadi, M.; Ahmadi, F. Determination of Homocysteine Using a Dopamine-Functionalized Graphene Composite. *Microchemical Journal* **2021**, *165*, 106124, doi:10.1016/j.microc.2021.106124.
41. Gorle, D.B.; Kulandainathan, M.A. Electrochemical Sensing of Dopamine at the Surface of a Dopamine Grafted Graphene Oxide/Poly(Methylene Blue) Composite Modified Electrode. *RSC Adv.* **2016**, *6*, 19982–19991, doi:10.1039/C5RA25541D.
42. Ghilane, J.; Hauquier, F.; Lacroix, J.-C. Oxidative and Stepwise Grafting of Dopamine Inner-Sphere Redox Couple onto Electrode Material: Electron Transfer Activation of Dopamine. *Anal. Chem.* **2013**, *85*, 11593–11601, doi:10.1021/ac402994u.

Preprints.org (www.preprints.org) | NOT PEER-REVIEWED | Posted: 21 February 2025 doi:10.20944/preprints202502.1766.v1

43. Rubianes, M.D.; Strumia, M.C. Polyethylenimine Functionalized with Dopamine: Characterization and Electrocatalytic Properties. *Electroanalysis* **2010**, *22*, 1200–1206, doi:10.1002/elan.200900552.
44. González-Romero, E.; González-Costas, J.; González-Veiga, M.C.; Carro-Pérez, I. Superficie Catalítica 2014. (Patent No. ES 2 389 936 B2). ES. Patent and Trademark Office. https://consultas2.oepm.es/pdf//ES/0000/000/02/38/99/ES-2389936_B2.pdf
45. Zollinger, H. *Diazo Chemistry*; VCH: Weinheim ; New York, 1994; ISBN 978-3-527-29213-4.
46. García-González, R.; Fernández-Abedul, M.T.; Pernía, A.; Costa-García, A. Electrochemical Characterization of Different Screen-Printed Gold Electrodes. *Electrochimica Acta* **2008**, *53*, 3242–3249, doi:10.1016/j.electacta.2007.07.059.
47. Laurentius, L.; Stoyanov, S.R.; Gusarov, S.; Kovalenko, A.; Du, R.; Lopinski, G.P.; McDermott, M.T. Diazonium-Derived Aryl Films on Gold Nanoparticles: Evidence for a Carbon–Gold Covalent Bond. *ACS Nano* **2011**, *5*, 4219–4227, doi:10.1021/nn201110r.
48. Berisha, A.; Combellas, C.; Kanoufi, F.; Médard, J.; Decorse, P.; Mangeney, C.; Kherbouche, I.; Seydou, M.; Maurel, F.; Pinson, J. Alkyl-Modified Gold Surfaces: Characterization of the Au–C Bond. *Langmuir* **2018**, *34*, 11264–11271, doi:10.1021/acs.langmuir.8b01584.
49. Kesavan, S.; Abraham John, S. Spontaneous Grafting: A Novel Approach to Graft Diazonium Cations on Gold Nanoparticles in Aqueous Medium and Their Self-Assembly on Electrodes. *Journal of Colloid and Interface Science* **2014**, *428*, 84–94, doi:10.1016/j.jcis.2014.04.038.
50. Blacha-Grzechnik, A.; Turczyn, R.; Burek, M.; Zak, J. In Situ Raman Spectroscopic Studies on Potential-Induced Structural Changes in Polyaniline Thin Films Synthesized via Surface-Initiated Electropolymerization on Covalently Modified Gold Surface. *Vibrational Spectroscopy* **2014**, *71*, 30–36, doi:10.1016/j.vibspec.2014.01.008.
51. Wang, J.; Carlisle, J.A. Covalent Immobilization of Glucose Oxidase on Conducting Ultrananocrystalline Diamond Thin Films. *Diamond and Related Materials* **2006**, *15*, 279–284, doi:10.1016/j.diamond.2005.09.017.
52. Gui, A.L.; Liu, G.; Chockalingam, M.; Le Saux, G.; Luais, E.; Harper, J.B.; Gooding, J.J. A Comparative Study of Electrochemical Reduction of 4-Nitrophenyl Covalently Grafted on Gold and Carbon. *Electroanalysis* **2010**, *22*, 1824–1830, doi:10.1002/elan.201000164.
53. Cullen, R.J.; Jayasundara, D.R.; Soldi, L.; Cheng, J.J.; Dufaure, G.; Colavita, P.E. Spontaneous Grafting of Nitrophenyl Groups on Amorphous Carbon Thin Films: A Structure–Reactivity Investigation. *Chem. Mater.* **2012**, *24*, 1031–1040, doi:10.1021/cm2030262.
54. Ortiz, B.; Saby, C.; Champagne, G.Y.; Bélanger, D. Electrochemical Modification of a Carbon Electrode Using Aromatic Diazonium Salts. 2. Electrochemistry of 4-Nitrophenyl Modified Glassy Carbon Electrodes in Aqueous Media. *Journal of Electroanalytical Chemistry* **1998**, *455*, 75–81, doi:10.1016/S0022-0728(98)00252-6.
55. Phal, S.; Shimizu, K.; Mwanza, D.; Mashazi, P.; Shchukarev, A.; Tesfalidet, S. Electrografting of 4-Carboxybenzenediazonium on Glassy Carbon Electrode: The Effect of Concentration on the Formation of Mono and Multilayers. *Molecules* **2020**, *25*, 4575, doi:10.3390/molecules25194575.
56. Fanjul-Bolado, P.; Hernández-Santos, D.; Lamas-Ardisana, P.J.; Martín-Pernía, A.; Costa-García, A. Electrochemical Characterization of Screen-Printed and Conventional Carbon Paste Electrodes. *Electrochimica Acta* **2008**, *53*, 3635–3642, doi:10.1016/j.electacta.2007.12.044.
57. Pinson, J.; Podvorica, F. Attachment of Organic Layers to Conductive or Semiconductive Surfaces by Reduction of Diazonium Salts. *Chem. Soc. Rev.* **2005**, *34*, 429, doi:10.1039/b406228k and references therein.
58. Wang, J. *Analytical Electrochemistry*; 1st ed.; Wiley, 2006; ISBN 978-0-471-67879-3.
59. Laviron, E. General Expression of the Linear Potential Sweep Voltammogram in the Case of Diffusionless Electrochemical Systems. *Journal of Electroanalytical Chemistry and Interfacial Electrochemistry* **1979**, *101*, 19–28, doi:10.1016/S0022-0728(79)80075-3.
60. Nicholson, R.S. Theory and Application of Cyclic Voltammetry for Measurement of Electrode Reaction Kinetics. *Anal. Chem.* **1965**, *37*, 1351–1355, doi:10.1021/ac60230a016.
61. Saleh, G.A.; Askal, H.F.; Refaat, I.H.; Naggar, A.H.; Abdel-aal, F.A.M. Adsorptive Square Wave Voltammetric Determination of the Antiviral Drug Valacyclovir on a Novel Sensor of Copper

Preprints.org (www.preprints.org) | NOT PEER-REVIEWED | Posted: 21 February 2025 doi:10.20944/preprints202502.1766.v1

Microparticles–Modified Pencil Graphite Electrode. *Arabian Journal of Chemistry* **2016**, *9*, 143–151, doi:10.1016/j.arabjc.2015.08.015.

62. Sui, L.; Wu, T.; Liu, L.; Wang, H.; Wang, Q.; Hou, H.; Guo, Q. A Sensitive Pyrimethanil Sensor Based on Electrospun TiC/C Film. *Sensors* **2019**, *19*, 1531, doi:10.3390/s19071531.
63. Vilà, N.; Bélanger, D. Mixtures of Functionalized Aromatic Groups Generated from Diazonium Chemistry as Templates towards Bimetallic Species Supported on Carbon Electrode Surfaces. *Electrochimica Acta* **2012**, *85*, 538–547, doi:10.1016/j.electacta.2012.08.035.
64. Bouden, S.; Bellakhal, N.; Chaussé, A.; Dachraoui, M.; Vautrin-Ul, C. Correlations between the Grafting Conditions and the Copper Detection by Diazonium Functionalized Carbon Screen-Printed Electrodes. *Electrochimica Acta* **2014**, *125*, 149–155, doi:10.1016/j.electacta.2014.01.083.
65. Brooksby, P.A.; Downard, A.J. Electrochemical and Atomic Force Microscopy Study of Carbon Surface Modification via Diazonium Reduction in Aqueous and Acetonitrile Solutions. *Langmuir* **2004**, *20*, 5038–5045, doi:10.1021/la049616i and references therein.
66. Kumar, A.S.; Sornambikai, S.; Gayathri, P.; Zen, J.-M. Selective Covalent Immobilization of Catechol on Activated Carbon Electrodes. *Journal of Electroanalytical Chemistry* **2010**, *641*, 131–135, doi:10.1016/j.jelechem.2009.12.016.
67. Smanhotto Malvessi, G.; Dannehl Hoppe, T.; Zapp, E.; Brondani, D. Lab-Made Screen-Printed Electrode with Conductive Ink Based on Carbon Nanomaterials for Simultaneous Electrochemical Analysis of Bisphenol A, Catechol, and 4-Nitrophenol. *Measurement* **2024**, *231*, 114601, doi:10.1016/j.measurement.2024.114601.
68. De Oliveira, S.P.; De Oliveira Cândido, T.C.; Pereira, A.C.; Da Silva, D.N. Electrochemical Determination of Catechol Using a Disposable Printed Electrode with Conductive Ink Based on Graphite and Carbon Black. *Analytica* **2024**, *5*, 250–262, doi:10.3390/analytica5020016.
69. Manoj, D.; Gnanasekaran, L.; Rajendran, S.; Jalil, A.A.; Siddiqui, M.N.; Gracia, F.; Soto-Moscoso, M. A Mechanothermal Approach for the Synthesis of Fe3O4 Nanoparticles as Dopant on Mesoporous TiO2 for Electrochemical Determination of Catechol. *Environmental Research* **2023**, *222*, 115358, doi:10.1016/j.envres.2023.115358.
70. Zhao, L.; Yu, J.; Yue, S.; Zhang, L.; Wang, Z.; Guo, P.; Liu, Q. Nickel Oxide/Carbon Nanotube Nanocomposites Prepared by Atomic Layer Deposition for Electrochemical Sensing of Hydroquinone and Catechol. *Journal of Electroanalytical Chemistry* **2018**, *808*, 245–251, doi:10.1016/j.jelechem.2017.12.019.
71. Gao, Z.-Y.; Gao, Y.-L.; Wang, E.; Xu, S.; Chen, W. Electrochemical Determination of Catechol Based on Cadmium Telluride Quantum Dots/Graphene Composite Film Modified Electrode. *J. Electrochem. Soc.* **2016**, *163*, H528–H533, doi:10.1149/2.0681607jes.
72. Xu, G.; Tang, B.; Jing, S.; Tao, J. Simultaneous Determination of Hydroquinone, Catechol and Resorcinol at Poly(3-Thiophenemalonic Acid) Modified Glassy Carbon Electrode. *International Journal of Electrochemical Science* **2015**, *10*, 10659–10667, doi:10.1016/S1452-3981(23)11289-2.
73. Hu, F.; Chen, S.; Wang, C.; Yuan, R.; Yuan, D.; Wang, C. Study on the Application of Reduced Graphene Oxide and Multiwall Carbon Nanotubes Hybrid Materials for Simultaneous Determination of Catechol, Hydroquinone, p-Cresol and Nitrite. *Analytica Chimica Acta* **2012**, *724*, 40–46, doi:10.1016/j.aca.2012.02.037.
74. Pérez-López, B.; Merkoçi, A. Magnetic Nanoparticles Modified with Carbon Nanotubes for Electrocatalytic Magnetoswitchable Biosensing Applications. *Adv. Funct. Mater.* **2011**, *21*, 255–260, doi:10.1002/adfm.201001306.
75. Zhang, Y.; Wang, Y.; Zhang, Z.; Sobhy, A.; Sato, S.; Uchida, M.; Hasebe, Y. Natural Molybdenite- and Tyrosinase-Based Amperometric Catechol Biosensor Using Acridine Orange as a Glue, Anchor, and Stabilizer for the Adsorbed Tyrosinase. *ACS Omega* **2021**, *6*, 13719–13727, doi:10.1021/acsomega.1c00973.
76. Chen, L.; Gu, B.; Zhu, G.; Wu, Y.; Liu, S.; Xu, C. Electron Transfer Properties and Electrocatalytic Behavior of Tyrosinase on ZnO Nanorod. *Journal of Electroanalytical Chemistry* **2008**, *617*, 7–13, doi:10.1016/j.jelechem.2008.01.009.
77. Wong, A.; Santos, A.M.; Fatibello-Filho, O.; Sotomayor, M.D.P.T. Amperometric Tyrosinase Biosensor Based on Carbon Black Paste Electrode for Sensitive Detection of Catechol in Environmental Samples. *Electroanalysis* **2021**, *33*, 431–437, doi:10.1002/elan.202060084.

Preprints.org (www.preprints.org) | NOT PEER-REVIEWED | Posted: 21 February 2025 doi:10.20944/preprints202502.1766.v1

78. Camargo, J.R.; Silva, T.A.; Rivas, G.A.; Janegitz, B.C. Novel Eco-Friendly Water-Based Conductive Ink for the Preparation of Disposable Screen-Printed Electrodes for Sensing and Biosensing Applications. *Electrochimica Acta* **2022**, *409*, 139968, doi:10.1016/j.electacta.2022.139968.
79. Vicentini, F.C.; Janegitz, B.C.; Brett, C.M.A.; Fatibello-Filho, O. Tyrosinase Biosensor Based on a Glassy Carbon Electrode Modified with Multi-Walled Carbon Nanotubes and 1-Butyl-3-Methylimidazolium Chloride within a Dihexadecylphosphate Film. *Sensors and Actuators B: Chemical* **2013**, *188*, 1101–1108, doi:10.1016/j.snb.2013.07.109.
80. Cagnani, G.R.; Ibáñez-Redín, G.; Tirich, B.; Gonçalves, D.; Balogh, D.T.; Oliveira, O.N. Fully-Printed Electrochemical Sensors Made with Flexible Screen-Printed Electrodes Modified by Roll-to-Roll Slot-Die Coating. *Biosensors and Bioelectronics* **2020**, *165*, 112428, doi:10.1016/j.bios.2020.112428.
81. Lu, Z.; Wang, Y.; Zhang, Z.; Shen, Y.; Li, M. Tyrosinase Modified Poly(Thionine) Electrodeposited Glassy Carbon Electrode for Amperometric Determination of Catechol. *Electrochemistry* **2017**, *85*, 17–22, doi:10.5796/electrochemistry.85.17.

Disclaimer/Publisher's Note: The statements, opinions and data contained in all publications are solely those of the individual author(s) and contributor(s) and not of MDPI and/or the editor(s). MDPI and/or the editor(s) disclaim responsibility for any injury to people or property resulting from any ideas, methods, instructions or products referred to in the content.